Petrogenesis of post-collisional Middle Eocene volcanism in the Eastern Pontides (NE, Turkey): Insights from geochemistry, whole-rock Sr-Nd-Pb isotopes, zircon U-Pb and 40Ar-39Ar geochronology

Emre Aydinçakir, Cem Yücel, Gilles Ruffet, Mehmet Ali Gücer, Enver Akaryali, Abdullah Kaygusuz, Mehmet Gücer

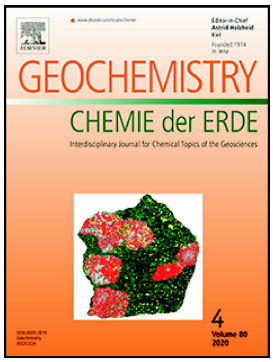

Petrogenesis of post-collisional Middle Eocene volcanism in the Eastern Pontides (NE, Turkey): Insights from geochemistry, whole-rock Sr-Nd-Pb isotopes, zircon U-Pb and 40Ar-39Ar geochronology

Emre Aydınçakır, Cem Yücel, Gilles Ruffet, Mehmet Ali Gücer, Enver Akaryalı, Abdullah Kaygusuz

PII: S0009-2819(22)00011-3

DOI: https://doi.org/10.1016/j.chemer.2022.125871

Reference: CHEMER 125871

To appear in: *Geochemistry*

Received date: 16 August 2021

Revised date: 15 February 2022

Accepted date: 17 February 2022

Please cite this article as: E. Aydınçakır, C. Yücel, G. Ruffet, et al., Petrogenesis of post-collisional Middle Eocene volcanism in the Eastern Pontides (NE, Turkey): Insights from geochemistry, whole-rock Sr-Nd-Pb isotopes, zircon U-Pb and 40Ar-39Ar geochronology, *Geochemistry* (2021), https://doi.org/10.1016/j.chemer.2022.125871

Petrogenesis of Post-Collisional Middle Eocene Volcanism in the Eastern Pontides (NE, Turkey): Insights from Geochemistry, Whole-rock Sr-Nd-Pb isotopes, Zircon U-Pb and ^{40}Ar-^{39}Ar geochronology

Emre Aydınçakır[1], Cem Yücel[2, 3], Gilles Ruffet[3,4], Mehmet Ali Gücer[1], Enver Akaryalı[1], Abdullah Kaygusuz[1]

[1]*Department of Geological Engineering, Gümüşhane University, TR-29100, Gümüşhane, Turkey*

[2]*Department of Mining Engineering, Gümüşhane University, TR-29100, Gümüşhane, Turkey*

[3]*CNRS (CNRS/INSU) UMR6118, Géosciences Rennes, Université de Rennes1, F-35042 Rennes Cedex, France*

[4]*Université de Rennes1, Géosciences Rennes, F-35042 Rennes Cedex, France*

Abstract

The debate about whether Eocene magmatism is considered to be post-collisional or subduction-related or not still continues. Here we offer new ^{40}Ar-^{39}Ar ad U-Pb zircon geochronology, mineral chemistry, bulk rock and Sr-Nd-Pb isotope geochemistry data obtained from the southern dike (SD) suite, in comparison with the northern dike (ND) suite, from the Eastern Pontides. The geochronological data indicate that the SD suite erupted between 45.89 and 45.10 Ma corresponding to the Lutetian (Middle Eocene). The magmas of the ND suite are characterised by slightly more alkaline affinity compared to the SD suite. The trace and rare earth element (REEs) content of the SD suite is characterised by large ion lithophile element (LILEs; Sr, K_2O, Ba, Rb) enrichment and depletion of Nb, Ta, and TiO_2 elements to different degree with high Th/Yb ratios, which indicate that the magmas forming

the SD and ND suites were derived from lithospheric mantle sources enriched by mostly slab-derived fluids in the spinel stability field. The Sr, Nd and Pb radiogenic isotope ratios of the dikes support the view that the magma for the hydrous group (H-SD) was derived from a relatively more enriched mantle source than the other SD and ND suites. The ND suite and the anhydrous group (A-SD) display similar geochemical features characterised by moderate light earth element (LREE)/heavy rare earth element (HREE) ratios, while the H-SD group has respectively lower LREE/HREE ratios indicating higher melting degree. Detailed considerations of the alkalinity, enrichment and partial melting degree for the source of the studied volcanic rocks indicate that the magmas of the northern dike suite are characterised by slightly more alkaline affinity, whereas the magmas throughout the southern dike suite show increments in the enrichment rate and melting degree. In light of the obtained data and comparative interpretations, the geodynamic evolution and differences in petrogenetic character of the Lutetian magmas from both the northern and southern parts of the Eastern Pontides may be explained by different degrees of melting of a net veined mantle source initially metasomatized by mostly subduction fluids during asthenospheric upwelling due to fragmented asymmetric delamination in a post-collisional extensional tectonic environment.

Keywords: U-Pb geochronology, ^{40}Ar-^{39}Ar thermochronology, Sr-Nd-Pb isotopes, net veined mantle, delamination, Eastern Pontides, Turkey

1. Introduction

The Eastern Pontide orogenic belt is located in the eastern Sakarya Zone (Northern Turkey, Fig. 1a) and can be accepted as one of the most complex and significant parts of the Alpine-Himalayan system due to consecutive subduction and collision events. From past to present, many authors studied on the geodynamic evolution of the region (e.g., Şengör and Yılmaz 1981; Bektaş, 1987; Genç and Yılmaz 1995; Okay and Şahinturk 1997;Yılmaz et al.

1997; Arslan et al. 1997; Altherr et al. 2008; Arslan and Aliyazicioglu 2001; Temizel and Arslan 2009; Aslan 2010; Temizel et al. 2012; Kaygusuz et al. 2011; Arslan et al 2013; Yücel et al. 2014a, b Temizel et al. 2016; Aydınçakır 2012; Aydınçakır and Şen 2013; Yücel 2017; Yücel et al., 2017; Temizel et al. 2019; Yücel 2019). Understanding the characteristics of Lutetian (Middle Eocene) magmatism is essential for interpretation of the geodynamic evolution of the region because of ongoing debate about whether magmatism was subduction-related or post-collisional resulting from the collision of the Anatolide-Tauride block with the Pontides during the closure of the northern branch of the Neo-Tethys Ocean.

Dikes are the efficient mechanisms that transport high volume of magmas through the crust. Studies related to the dikes have attracted the attention of many geologists for a long time and they have a key role in geodynamic interpretation as well. The dikes in regions like the Eastern Pontides are characterised by dominant pyroclastic volcanic rocks compared to lavas especially in the Eocene era. It is of key importance to collect reliable samples from a certain time gap, in addition to their structural importance to understand the tectonic evolution of the region. This study aims to assess source mineralogy, enrichment processes, and melting mechanism in the source area for Tertiary magmas in basic-intermediate dikes from the Eastern Pontides orogenic belt. We utilised new information about major, trace and rare earth elements, geochronological and isotope data from the southern part of the Eastern Pontides with comparative petrology of dikes from the northern part of the region (initially presented by Yücel et al. 2017). Based on the data presented here, the aim was to contribute to a better interpretation of petrogenetic processes and their possible geodynamic significance for Eocene magmatism.

2. Geological Setting and Local Geology

Sakarya Zone is ribbon continent and situated in the north of Turkey extending from the Biga Peninsula to Lesser Caucasus. This tectonic unit comprises a mountain chain 200 km wide and 500 km long and is accepted as a part of the Alpine orogenic system. Igneous records documenting the active margin of the Neo-Tethyan convergence system were followed by the collision of the Eastern Pontides and the Tauride-Anatolide platform (Şengör and Yılmaz, 1981). The Carboniferous granitoids intruded into the pre-basement rocks in the Eastern Pontides (Fig. 1b) (e.g., Topuz et al., 2010; Dokuz, 2011; Nikishin et al., 2015; Dokuz et al., 2015; Kaygusuz et al., 2012, 2016). Late Carboniferous to Early Permian sedimentary rocks, indicating a shallow marine environment, unconformably overlie the basement rocks (Çapkınoğlu, 2003; Topuz et al., 2007; Kandemir and Yerosey-Aubril 2011). Late Triassic lamprophyres crosscut the Palaeozoic basement in the southern part of the Eastern Pontides (e.g. Dokuz et al., 2010; Karsli et al., 2014). In the southern part, Early and Middle Jurassic basic volcanic and sedimentary rocks lie unconformably on the basement rocks (e.g., Şengör and Yilmaz, 1981; Dokuz and Tanyolu 2006; Kandemir and Yilmaz, 2009;). The Jurassic granitoids and their volcanic equivalents cross-cut the Şenköy Formation comprising volcanoclastic and sedimentary rocks (Dokuz et al., 2010; Dokuz et al 2017; Aydınçakır et al., 2020) and they are conformably overlain by the Upper Jurassic to Cenomanian Berdiga Formation characterised by carbonate dominant sediments (Pelin, 1977) (Fig. 2a, b). In the southern part, these units are unconformably covered by Late Cretaceous sedimentary rocks in some locations (e.g., Yılmaz and Korkmaz 1999), whereas the volcanic rocks of the same age with tholeiitic to calc-alkaline affinity occur in the northern part (Çamur et al., 1996; Arslan et al., 1997; Aydınçakır, 2016). Late Cretaceous granitoids intrude into these units (e.g., Kaygusuz and Aydinçakir 2011; Karsli et al., 2018; Temizel et al., 2019). Additionally, geochronologic studies about high to ultrahigh potassic rocks from the western end of the Eastern Pontides indicating Late Cretaceous age were reported by many authors (Asan et al.,

2014; Eyüboğlu, 2010; Genç et al., 2014; Gülmez and Genç 2015; Aydınçakır, 2016, Gülmez et al., 2017). Post-Cretaceous magmatism starts with Palaeocene plagioleucitites in the southern part of the Eastern Pontides (Altherr et al., 2008). The transition of the Palaeocene–Early Eocene is another matter of debate in the Eastern Pontides. The existing studies by many researchers indicate that Eocene volcanism developed based on post-collisional processes according to geochemical characteristics (Okay and Şahintürk 1997; Boztuğ et al., 2004). The formation of adakitic volcanism in the Palaeocene - Early Eocene in the region is explained by two different mechanisms; (i) partial melting of the mafic crust during collision (e.g., Topuz et al., 2005; Karsli et al., 2010) or (ii) partial melting of an oceanic slab (e.g., Eyuboglu et al., 2011; Dokuz et al., 2013). The Eocene era is represented by volcanic and volcaniclastic rocks and they overlie the Late Cretaceous series in the southern part (Arslan and Aliyazicioglu 2001; Kaygusuz et al., 2011; Arslan et al., 2013; Aslan et al., 2014; Aydınçakır, 2014; Kaygusuz and Şahin 2014; Temizel et al., 2016). In the northern part, the Middle Eocene volcanic rocks are composed of basic to intermediate pyroclastic rocks, minor amounts of lava flows and dikes. These units were intruded by calc-alkaline granitoids of the same age (Arslan and Aslan 2006; Kaygusuz and Öztürk 2015; Dokuz et al., 2019; Fig. 1b). The Miocene volcanic history of the Eastern Pontides is less extensive and their affinity ranges from calc-alkaline to moderately alkaline, mainly reported in the Trabzon (Arslan et al., 1997; Aydin et al., 2008; Yücel et al., 2014, 2017) and the Ulubey (Ordu) areas in the northern part (Temizel et al., 2012) and the Gümüşhane area in the southern part (Arslan et al. 2013; Aslan et al. 2014). In the southern part of the Eastern Pontides, the Late Miocene adakitic rocks are dacite in composition (Eyuboglu et al., 2012a; Dokuz et al., 2013). The Late Miocene–Pleistocene volcanic rocks outcropping north of the North Anatolian Fault Zone (NAFZ) are represented by basalt and andesite (Karsli et al., 2008; Ekici, 2016), and

adakitic andesites (Yücel, 2019). The Miocene–Quaternary volcanic rocks in the Eastern Pontides were covered by Quaternary alluvium throughout the region.

The study area is situated in the southern part of the Eastern Pontide Orogenic Belt (Fig. 2a, b). The oldest rocks in the study area are Early-Middle Jurassic volcaniclastic rocks (Kandemir, 2004; Kandemir and Yılmaz, 2009). These rift-related volcanoclastic rocks are characterised by two main phases (Eyuboglu et al., 2006). The basic-intermediate volcanic and coarse clastic rocks represent the first phase. The second phase is represented by alternations of volcanic and epiclastic rocks (Eyuboglu et al., 2006). The Ammonitico Rosso-type pelagic limestones, showing short-term thermal subsidence in the region, are located between these two main phases. These units are covered by Late Jurassic-Lower Cretaceous carbonates in the whole Gümüşhane region (Fig. 2a, b). The Late Cretaceous rocks are characterised by a thick sedimentary sequence. The basement of this unit comprises yellowish sandy limestones. The red pelagic limestones overlie these and the sequence continues with sandstone, siltstone, claystone, marl and limestone alternations. In some places, they are interbedded with tuff. The Mesozoic units are crosscut by Lower Eocene adakitic stocks (Karsli et al., 2010a; Eyüboğlu et al., 2011; Dokuz et al., 2013). The whole units are unconformably covered by the Eocene series containing conglomerate and nummulite-bearing limestone at the bottom and passing to volcanic clastic rocks including basalt, andesite and associated pyroclastics toward the top. They are generally intruded by Eocene granitic plutons (Arslan and Aliyazıcıoglu, 2001; Arslan and Aslan, 2006; Arslan et al., 2013; Eyuboglu et al., 2017; Kaygusuz et al., 2019). The Eocene volcanic sequence is usually crosscut by 10 to 150 cm wide Eocene basaltic dikes (Fig. 2b), namely the southern dike (SD) suites which are the main topic of this study, representing the final stage of Middle Eocene magmatism. The dikes are fresh and have massive structures with nearly NW-SE orientations.

3. Analytical Methods

3.1. Geochronology

3.1.1. Ar-Ar Dating

Three groundmass fragments from hydrous and anhydrous series of the studied dikes were selected for ^{39}Ar-^{40}Ar dating. The analyses were conducted by the continuous laser probe (CO_2 Synrad®) stepwise heating technique and the isotopic contents were determined by using a Map215® mass spectrometer at the Geochronology laboratory of Rennes1 University (France). The detailed information about the analytical procedure can be found in the Supplementary Text 1.

3.1.2. U-Pb Dating

The U-Pb dating analysis on zircon grains extracted from the basaltic trachyandesite dike sample (B37; coordinate; 371 355752E 4474257N) was carried out by LA-MC-ICP-MS at the Arizona Laser Chron Center (Gehrels et al., 2008). The detailed information about the analytical procedure can be found in the Supplementary Text 1.

3.2. Whole-Rock Geochemistry

The 14 representative and freshest volcanic rock samples from the both A-SD and H-SD groups were determined for bulk rock analyses. Their major and trace element analyses were determined by ICP-AES and REE were measured by ICP-MS at the commercial ACME

Analytical Laboratories Ltd, in Vancouver, Canada. The detailed information about the analytical procedure can be found in the Supplementary Text 1.

3.3. Sr-Nd-Pb Isotope Geochemistry

The 7 representative samples from both hydrous and anhydrous series of the studied dikes were selected for Sr, Nd and Pb isotopic analyses. The analyses were performed by TIMS, on a VG Sector 30 mass spectrometer at the Analytical Geochemistry Research Laboratory at the New Mexico State University. The further information about the analytical procedure can be found in Ramos (1992) and in the Supplementary Text 1.

4. Results

4.1. Petrography

Phenocryst assemblage and modal mineralogy of the representative samples from the SD suite indicate that the studied volcanic rocks can be summarised in two groups: (1) anhydrous group (A-SD) represented by pl +cpx ± ol + opq minerals with microlithic porphyritic, hyalo-microlithic porphyritic, and glomeroporphyritic textures and (2) hydrous group (H-SD) represented by pl + hbl ± sa + opq minerals with flow, microlithic porphyritic, glomeroporphyritic, and poikilitic textures (Table 1). Basic samples of ND suite generally compose ol + cpx + pl ± bt ± hbl + opq minerals, whereas the intermediate samples are represented by pl + bt + cpx ± hbl ± sa + opq mineral combination with porphyritic textures (Yücel et al. 2014a). The phenocryst content is up to 25% for both groups in SD and the dominant mineral phase is plagioclase and clinopyroxenes for the anhydrous group, whereas plagioclase and hornblende are dominant mineral phases for the hydrous group. Additionally,

textural features such as sieve texture, slight zoning, resorbed and overgrowth rims observed in plagioclases and resorption of anhedral clinopyroxenes indicate that disequilibrium crystallization can be accepted as an effective process as well as fractional crystallization during the evolution of the anhydrous group volcanic rocks (Fig. 3).

4.2. Geochronology

The geochronology of the studied SD suite, cross-cutting the Early Eocene and Middle Eocene volcanic rocks in the southern part of the Eastern Pontides, was determined by using U-Pb and $^{40}Ar/^{39}Ar$ methods.

4.2.1. U-Pb Dating

The results of U-Pb zircon dating of the studied SD suite are presented in Supplementary Table 1 and corresponding concordia diagrams are summarised in Fig. 4a, b. The four separated zircon grains are almost clear and have concentric zoning indicating magmatic origin. Few grains show small cracks. The analysed zircon grains were mostly characterised by low Th and U concentrations varying from 18.9 ppm to 239.2 ppm and 15.9 ppm to 238.6 ppm, respectively and U/Th ratio is in range of 0.8 and 3.1. All dated zircon grains yielded concordant ages. The total of 6 spots from 3 zircon grains from B37 of the SD suite yielded $^{206}Pb/^{238}U$ concordia age of 45.89 ± 1.1 Ma with a weighted mean age of 45.95 ± 0.7 Ma (MSWD = 0.95). A Middle Eocene (Lutetian) age was established by U–Pb zircon dating. This is interpreted as the crystallization age for the H-SD group.

4.2.2. Ar-Ar Dating

The $^{40}Ar/^{39}Ar$ laser probe step heating method was used to determine the cooling age of the studied SD suite. The analyses were performed on groundmass fragments from both the A-SD and H-SD groups. The step heating experiment results are given as age spectra in Fig 4c, e and the age spectra and their inverse isochronous calculation ($^{36}Ar/^{40}Ar$ versus $^{39}Ar_K/^{40}Ar$; Turner, 1971; Roddick et al., 1980; Hanes et al., 1985) results are presented in Supplementary Table 2. Most of the age spectra for studied dike samples have flat patterns corresponding to more than 80% of the degassed $^{39}Ar_K$. The observed low and higher but decreasing apparent ages are most probably related to degassing of some weathering phase and limited $^{39}Ar_K$ recoil during irradiation, respectively. The volcanic rocks samples yielded 45.8 ± 0.1 Ma for H-SD suite and 45.1 ± 0.2 Ma for the A-SD suite corresponding to Middle Eocene (Lutetian). The $^{36}Ar/^{40}Ar$ dating results show that the A-SD suite could occur after the H- SD suite by about 0.7 Ma.

In the northern part, by using $^{40}Ar/^{39}Ar$ geochronology, Yücel et al. (2017) argued that the samples of the ND suite yielded ages of 45.31 ± 0.18 to 43.86 ± 0.19 Ma. Intermediate samples from the ND suite yielded ages of 44.87 ± 0.22 Ma to 41.32 ± 0.12 Ma corresponding to Middle Eocene (Lutetian).

4.3. Petrochemistry

The bulk rock composition of the studied H-SD and A-SD groups from the southern part of the Eastern Pontides are presented in Table 2. The A-SD group from the Gümüşhane area are mainly basalt and basaltic andesite in composition, whereas the H-SD group is generally basaltic trachyandesite in composition based on the total alkali (Na_2O+K_2O) versus SiO_2 plot

suggested by Le Bas et al. (1986) (Fig 5a). In addition, the basalt and basaltic andesite samples plot in the subalkaline field, while the basaltic trachyandesites are located in the alkaline field determined by Irvine and Baragar (1971), except for one sample plotted in the subalkaline field. In the classification diagram of Winchester and Floyd (1976), all the samples from the SD suite are plotted in the andesite/basalt field (Fig. 5b) and characterised by moderate silica content varying in a narrow range between 50.48 and 53.79 wt.%, high Al_2O_3 (17.78-21.54 wt.%) and low Mg# (Mg#= MgO/(MgO + $Fe_2O_3^t$)) from 0.27 to 0.34. In the SiO_2 versus K_2O diagram of Ewart (1982), the H-SD group straddles the calc-alkaline and high-K calc-alkaline series field, whereas the A-SD group plotted in the tholeiitic and calc-alkaline series field (Fig. 5c) and all the samples are located the calc-alkaline field of the AFM diagram (Fig. 5d) suggested by Irvine and Baragar (1971). Harker type variation diagrams generally don't show similar and consecutive trends for the H-SD and A-SD groups (Fig. 6). The Na_2O, P_2O_5, K_2O, Rb, Hf and Ni contents show positive trends and CaO, TiO_2, Al_2O_3, Sc, Sr and Ta represent correlations with the increasing SiO_2 content, which was selected as differentiation index. The studied dikes display similar patterns on primitive mantle-normalised (Sun and McDonough, 1989) multi-element variation diagrams (Fig. 7a). In the primitive mantle-normalised multi element diagram, the SD suite is characterised by enrichment in large-ion lithophile elements (LILEs; Sr, K, Ba, Rb), and Th, Ce and some high field strength elements (HFSEs; Zr, Ti, Y, Nb, Ta) are depleted, which is accepted as typical subduction zone signature. The H-SD group shows more elevated normalization values than the A-SD group, except for Sr. In chondrite-normalised (Taylor and McLannen, 1985) rare earth element (REE) diagrams, the studied dike samples are represented by two different straight and sub parallel trends (Fig 7b). The H-SD group shows more enriched pattern in LREEs than the A-SD group, leading to a steeper trend than the A-SD group, with La_N/Yb_N ratios varying between 2.22 and 2.87 for the A-SD group and 3.97 and 5.47 for the H-SD

group. For both the A-SD and H-SD groups have insignificant Eu anomaly varying from 0.89 to 0.96 and 0.99 to 1.12, respectively.

The ND suite was classified by using a TAS diagram with the basic samples of the ND generally basalt, trachybasalt, basaltic trachyandesite and trachyandesite in composition, whereas the intermediate samples are trachyandesite and trachyte in composition (Fig. 5a). They show calc-alkaline to shoshonitic affinity on the SiO_2 versus K_2O diagram (Fig. 5c) and they are characterised by typical calc-alkaline trend on the AFM diagram (Fig 5d). In the primitive mantle-normalised (Sun and McDonough, 1989a, 1989b) multi-element diagrams (Fig. 7a), both groups of ND suites show broadly similar patterns to the SD suite. The ND suite displays enriched REE patterns on chondrite-normalised REE diagrams (Fig. 7b). The enrichment in LREEs (La = 21–91, 35–113) and HREEs (Yb =3–10, 7–14) for the basic and intermediate groups of the ND suite resulted in La_N/Lu_N ratios ranging from 5.55–10.76 and 4.65–11.64, respectively (Yücel et al. 2017).

4.4. Sr-Nd-Pb Isotope Geochemistry

Sr-Nd-Pb isotope data for the studied SD suite are reported in Table 3 and the initial ratios of Sr and Nd isotopes were obtained by using crystallisation ages (~45 Ma) of the SD series obtained from Ar-Ar and U-Pb dating analysis. The A-SD group is characterised by $^{87}Sr/^{86}Sr$ initial ratios of 0.70448 – 0.70482 and εNd initial values (-0.17) – (+1.87). The H-SD group has more radiogenic initial $^{87}Sr/^{86}Sr$ values than the A-SD group varying between 0.70516 and 0.70542 with εNd values of (+0.78) – (+0.94). The basic samples of the ND suite are characterised by $^{87}Sr/^{86}Sr$ initial ratios of 0.70389 – 0.70431 and εNd initial values (+1.81) – (+3.70), while the intermediate dikes yielded $^{87}Sr/^{86}Sr$ initial ratios of 0.70407 – 0.70424 and εNd initial values (+1.80) – (+2.76) (Yücel et al. 2017). As illustrated in the $(^{87}Sr/^{86}Sr)_i$

versus ($^{143}Nd/^{144}Nd)_i$ diagram showing the distribution of Eocene-aged volcanic rocks from the Eastern Pontides (Fig. 8a), the A-SD group displays a close relationship with the ND suite from the Trabzon area (Yücel et al, 2017), Torul volcanics (Kaygusuz et al 2011), Borçka volcanics (Aydınçakır and Şen, 2013) and southern part volcanic rocks (Arslan et al 2013), while the H-SD group shows similarities with the Kale adakites (Karslı et al 2010), the Torul volcanics (Kaygusuz et al 2011) and the southern part volcanic rocks (Arslan et al. 2013). The H-SD group exhibits non-radiogenic Pb isotope ratios (varying $^{206}Pb/^{204}Pb$ = 18.51-18.74; $^{207}Pb/^{204}Pb$ = 15.59-15.66; $^{208}Pb/^{204}Pb$ = 38.55-38.83), while the A-SD group has Pb isotopic ratios such as $^{206}Pb/^{204}Pb$ = 18.51-18.74; $^{207}Pb/^{204}Pb$ = 15.59-15.66; and $^{208}Pb/^{204}Pb$ = 38.55-38.83. The lead isotope ratios for the basic dikes of the ND suite display narrow ranges, e.g., $^{206}Pb/^{204}Pb$ = 18.72-18.79; $^{207}Pb/^{204}Pb$ = 15.63-15.67; and $^{208}Pb/^{204}Pb$ = 38.79-38.92 and the intermediate samples from the ND suite are in the range of $^{206}Pb/^{204}Pb$ = 18.78-18.80; $^{207}Pb/^{204}Pb$ = 15.64-15.67; and $^{208}Pb/^{204}Pb$ = 38.87-38.97 (Yücel et al., 2017; Fig. 8b, c).

5. Discussion

Here, we discuss the evolution of the dikes studied in the northern and southern parts of the Eastern Pontides in light of a series of processes ranging from metasomatism in the source area by fluids and/or melts related to the initial subduction event, partial melting processes and its degree in the metasomatized mantle source and combined processes subsequently occurring at crustal levels such as mixing, FC and AFC.

5.1. Age Constraints

In previous studies, the age relations of the studied volcanic rocks were determined based on volcano stratigraphic criteria, contact relationships and geochronological studies. In the light of the palaeontological observations based on microfossil contents of the sedimentary rocks below the volcanic units, the volcanic activity started in the Palaeocene and continued to Eocene time (Arslan and Aliyazıcıoğlu 2001). Karsli et al. (2010) reported the ages of the adakitic volcanic rocks as 47.40 ± 1.89 to 50.27 ± 1.46 Ma based on $^{40}Ar/^{39}Ar$ dating. In the same area, Eyüboğlu et al. (2013) reported the U-Pb zircon ages of the adakitic and non-adakitic volcanic rocks that are crosscut by the studied dikes as 48.71 ± 0.74 Ma, and 44.68 ± 0.84 Ma, respectively. Finally, the K-Ar age of the andesitic lava flows were suggested as between 37.62 ± 3.33 Ma (Middle Eocene) and 30.02 ± 2.84 Ma (Early Oligocene), but 15.80 ± 1.71 Ma (Middle Miocene) age was obtained for the basaltic dikes by Aslan et al. (2014).

5.2. Source Composition

Petrological models based on the trace element content can be used to determine the source mineralogy, extent, depth, and degree of partial melting. Shaw (1970) proposed a model to determine conditions of partial melting along with mineralogical and geochemical composition of the source area for magmas. The REE characteristics of the studied SD suite in comparison to the ND suite can help to constrain the mineralogy of the source area. The almost flat HREE patterns of the studied dike samples indicate a spinel-bearing mantle mineralogy possibly shallower than 85 km (McKenzie and O'Nions 1991; Robinson and

Wood, 1998; Klemme, 2004). The REE content of the dike samples characterised by lower La_N/Yb_N ratios vary between 2.22 and 2.87 for the A-SD group, 3.97 and 5.47 for the H-SD group and 4.75 and 11.49 for ND series, which can be explained by relatively higher and different partial melting degrees in the source (Yücel et al., 2017). The spinel-bearing mineralogy has a lower La/Yb ratio (Thirlwall et al. 1994; Shaw et al. 2003). HREEs strongly reside in the crystal structure of garnet. The garnet-bearing mantle mineralogy indicating deeper source is capable of producing melts that generally tend to have high Dy/Yb ratios (> 2.5), whereas a spinel-bearing source is characterised by lower Dy/Yb ratios (<1.5; Yang et al., 2012). Furthermore, the melts derived from spinel-bearing sources generally display Dy_N/Yb_N ratios lower than 1.06 (Blundy et al., 1998). Respectively, more primitive basic samples, with SiO_2 content generally lower than 52 wt.%, were selected to investigate the source composition of the SD and ND suites. The A-SD and H-SD groups have a similar range of Dy_N/Yb_N ratios varying from 0.95 to 1.19 and from 0.99 to 1.19, respectively, whereas the ND suite has this ratio between 1.01 and 1.53. In light of these data, the Dy_N/Yb_N ratios of the studied rocks indicate that mostly melting of spinel peridotite could produce the melts for the SD suite, while the melts for the ND suite were derived from a deeper source with mixed mineralogy of spinel and garnet. Yucel et al. (2017) suggested that the parental magmas of the ND suite were derived from a phlogopite-bearing spinel lherzolite source according to the results of petrological modelling. To determine the source mineralogy and make predictions about partial melting degree, the plots of Sm versus Sm/Yb and La/Yb versus Dy/Yb were also used (Fig. 9a, b). Both the SD and ND suites plot between the curves for amphibole-garnet lherzolite and spinel lherzolite in Fig. 9a, whereas they exhibit similarities to spinel-lherzolite in Fig. 9b. The LILE enrichment in the mantle source area is commonly related to the presence of hydrous and volatile-bearing minerals such as amphibole and phlogopite (Ionov et al. 1997). The ND suite and the H-SD group display high Rb/Sr ratios in the range

of 0.11-0.17 and 0.02-0.45 and Ba/Rb ratios of 6.54-20.44 and 3.83-11.48, respectively, indicating the presence of phlogopite in the source mineralogy as a hydrous phase. Low Rb/Sr ratios varying between 0 and 0.03 and Ba/Rb ratios varying between 21.63 and 261.67 for the A-SD group shows that amphibole was present as hydrous phase in the source mineralogy (Furman and Graham 1999; Fig. 9c). The decreasing Sm (ppm) content and La/Yb ratios in Fig. 9a and b are related to the increasing partial melting degree. The degree of the partial melting increases from the ND suite (0.01 to 5 and generally around 0.01; Yucel et al., 2017) to the H-SD (0.01 to 3 and generally around 3) and the A-SD (3-10 and generally around 5) groups based on the La/Yb versus Dy/Yb diagram (Fig. 9b).

Melting of a heterogeneous net veined mantle source including hydrous minerals with the coexisting surrounding peridotites to different degrees leads to generation of various alkaline and calc-alkaline melt types. The melting of vein-dominated mantle with lower melting degree leads to generation of alkaline melts, while the melting of the metasomatic domains accompanied by melting of surrounding peridotites with increased partial melting degree generates calc-alkaline, shoshonitic and high-K melts (e.g., Foley 1992; Prelević et al. 2008; 2012). Previous studies support the idea that this type of mantle source is probably present for both the entire Eastern Pontides (Yücel et al. 2017) and the Alpine-Himalayan system (Prelević et al. 2008). The melting degree in the source increases from north to south according to petrological modelling efforts and REE characteristics.

5.3. Role of Subduction Enrichment

The trace and REE content of the studied dikes reflects similarities with the subduction-related magmas characterised by LILE enrichment and HFSE depletion (Nb, Ta and Ti in particular). In general, these chemical properties of post-collisional magmas can be

interpreted as derivation from a mantle source modified by ancient subduction-related metasomatic enrichment induced by melts or fluids released from the subducted oceanic crust (e.g., Duncan et. al., 1984; Ewart et. al., 2004). The plot of Th/Yb versus Ta/Yb is capable of interpreting the variation in the source composition and whether crustal contamination is effective on the evolution of magmas or not (Pearce et al., 1990). In this diagram (Fig. 10a), the vertical shifts to higher Th/Yb ratios suggest the effect of subduction-induced fluids and/or melts, while the trends with high Th/Yb, parallel or subparallel to the mantle array can indicate FC and AFC processes. The geochemical signature of the studied dikes that plot above the mantle array with different Th/Yb ratios reflect characteristics of magmatic processes varying from FC to AFC that played roles in magma generation from a lithospheric mantle source modified by subduction-induced fluids and/or melts.

These types of features observed in post-collusional magmas can be consequences of metasomatism arising from previous subduction-related processes. In the literature, the fluids from the altered oceanic crust (e.g., Turner et al., 1996; Guo et al., 2005) or fluids and melts from subducted oceanic crust and sediments can be regarded as effective metasomatic components (e.g., Elburg et al., 2002). Some LILE elements (e.g., Ba, Rb, Sr, U) are mobile, while HFSEs and REEs are less mobile in the fluid-like component (Sheppard and Taylor, 1992; Turner et al. 1997; Turner, 2002). Moreover, magmas with a strong imprint of fluid-like metasomatism generally have higher Pb/Ce (> 0.1; Elburg et al., 2002), Ba/Th (> 170; Hawkesworth et al. 1997) and Ba/La ratios. Magmas strongly affected by subduction-related melts or subducted sediments in the source area are generally characterised by high Th/Ce ratios (> 0.15; Hawkesworth et al. 1997). The SD suite has fingerprints of a fluid-like component reflected by the high Ba/Th (216.2-893.3) ratio on the Ba/Th versus Th (ppm) diagram, while the ND suite (Yücel et al. 2017) possesses signatures for sediment or sediment melt character with high Th content (Figure 10b). The modifications in the source area by

melt or fluid-like metasomatic components can also be argued by using the Th/Yb and Ba/La ratios (Fig.10c). It is clearly indicated that Ba enrichment relative to La in the magmas of the SD suite is more distinguishable than the ND suite, and the SD suite carries more traces of a fluid-like component compared to the ND suite. The Sr/La ratio shows broad variation relative to the La/Yb ratio (Fig. 10d) so the sources of both the SD and ND suites were modified by fluid-like components. Additionally, source enrichment can be deduced by using the Ce/Pb systematics as well. Pb generally attracts attention to a fluid mobile character compared to Ce and thus, magmas derived from mantle source characterised by fluid-related metasomatism tend to have low Ce/Pb ratios (e.g., Miller et al. 1994; Chauvel et al. 1995). High Th/La ratios are observed for magmas derived from the melting of subducted continental sediments or crustal magmatic sources (Plank, 2005). The SD suite is characterised by low Ce/Pb and Th/La ratios, indicating fluid-like metasomatism in the source area, while the ND suite has low Ce/Pb and variable Th/La ratios, implying sediment activity or sediment melt (Fig. 10e). Moreover, the observed slightly lower $^{143}Nd/^{144}Nd$ ratio and slightly high $^{87}Sr/^{86}Sr$ ratio in the H-SD group with relatively more alkaline affinity than the A-SD group, makes sense if these dikes were derived from a respectively more enriched mantle source such as hydrous mineral-bearing net veined mantle. Therefore, the degree and type of enrichment in magmas from the SD suite differ from the ND suite.

5.4. Fractional Crystallization (FC) versus Crustal Contamination (AFC)

To interpret the behaviour of trace element content and isotopic ratios observed in the studied dikes, the role of FC and AFC processes needs to be considered. The SD series have element contents of MgO (2.56-4.71 wt.%), Cr (<65 ppm), Ni (1.9-5.0 ppm) as well as Mg number (0.27-0.34) that distinctively differ from primitive magmas (SiO_2<52 wt.%, MgO >

10 wt.%, Ni >200 ppm and Cr > 300 ppm, Mg number; e.g., Hart & Davis, 1978, Frey et al., 1978). The question is which possible magmatic processes, such as magma mixing, FC and/or AFC, played an effective role in the genesis of the magmas.

The samples from H-SD and A-SD groups do not generally represent consecutive trends indicating common magma source within the discrimination diagrams. In these diagrams, decreasing content of MgO, Fe_2O_3, CaO, TiO_2, Sc, and V with increasing silica content for the A-SD group indicated that fractionation of clinopyroxene and Fe-Ti oxides were effective and they were removed from the evolving melt. The Al_2O_3, CaO and Sr reductions may be explained by the fractionation of plagioclase. Moreover, the K/Rb versus Rb, Ba versus Sr and Sr versus MgO diagrams were used to determine fractionated mineral phases (Fig. 11a, b, c). In Fig. 11a, the strong decrease in the K/Rb ratio with increasing Rb indicates the crystallization of clinopyroxene in the A-SD group whereas the horizontal variations of K/Rb with increasing Rb implies the crystallization of a hydrous Mg-K bearing phase, such as hornblende, for the H-SD group. On the Ba versus Sr diagram, an increase in Ba with the decrease in Sr indicates the fractionation of plagioclase in both the A-SD and H-SD groups (Fig. 11b). However, the fractionation of plagioclase might not play an important role based on the slight, and lack of Eu anomalies (Eu/Eu* 0.79 to 1.12) for all the SD suites. The increase and decrease of Sr with decreasing MgO reflects clinopyroxene and plagioclase fractionation, respectively, in Fig. 11c. The A-SD group is characterised by the crystallisation of clinopyroxene, but plagioclase fractionation is not important at all for both groups in the SD suite (Fig. 11c). Yücel et al. (2017) stated that the Harker diagrams for the basic and intermediate dikes of the ND suite indicate a significant role of fractional crystallization during the evolution of their magmas. The observed positive and negative trends in the Harker diagrams for the ND suite are probably related to olivine, clinopyroxene, Fe-Ti oxides, plagioclase, phlogopite, K-feldspar and apatite fractionation.

As was pointed out by geochemical variations and bivariate graphs with highly incompatible/compatible element pairs, the SD suite might have evolved by the effect of fractional crystallisation. In this part, the modelled fractional crystallisation trends were created to examine which mineral phases participated in the fractional crystallisation processes by using Keskin (2002)'s FC model program. For the fractional crystallization modelling, Co was selected as compatible element for many ferromagnesian minerals and Th was selected as highly incompatible element for many mineral groups. The most basic sample (B24) from the A-SD group was selected as the starting composition. Five different theoretical curves were created by using mineral proportions in different rates. The data for the SD suite plotted on the Co versus Th FC modelling diagram indicates that the studied dikes track curves 1 and 5 which almost coincide (Fig. 11d). The harmonic behaviour between samples and the modelled vectors show that clinopyroxene, hornblende and plagioclase are the dominant phases (~15%, amp, ~50% pl, ~35-50% cpx). These results from geochemical modelling and detailed petrographic observations have some similarities, supporting fractionation of these mineral phases. According to the FC modelling efforts for basic dikes of the ND suite, clinopyroxene (~40–50%) and plagioclase (~50%) are the dominant phases and a minor amount of olivine (~10%) accompanies these assemblages (Yücel et al. 2017). The intermediate samples from the ND suite were characterised by fractionated mineral phases of plagioclase (~55%) and amphibole (~30%) with minor amounts of clinopyroxene, biotite and sanidine (~5%, ~5% and ~5%, respectively).

The geochemical and isotopic budget of the studied dikes can be used to interpret the magmatic processes responsible for the evolution of the volcanic rocks including fractional crystallization and crustal contamination. The samples from H-SD and A-SD groups have low MgO and Mg# values that Show the effect of AFC besides FC.

The significant role of crustal assimilation can be determined based on whether there is a correlation between the isotopic ratio and major elements or not. Fig. 12a and b were created by using the $(^{87}Sr/^{86}Sr)_i$, $(^{143}Nd/^{144}Nd)_i$ ratios and SiO_2 content. In these diagrams, effect of crustal assimilation was determined due to the correlation between $(^{87}Sr/^{86}Sr)_i$, $(^{143}Nd/^{144}Nd)_i$ ratio, and SiO_2 content of the SD suite, and the ND suite (Fig. 12a, b). Fractional crystallization and assimilation processes are significant for the evolution of both SD and ND suites (Fig. 12a, b). In the $(Th/Yb)_{PM}$ versus $(Nb/Yb)_{PM}$ diagram (Fig. 12c), the primitive mantle (PM) normalised ND suite displays similar variation with the crustal contamination arrow for low $(Nb/Yb)_{PM}$ and high $(Th/Yb)_{PM}$ contents. The SD suite shows similar trends to crustal contamination. The data plotted in Fig. 12d also support the view that AFC is not significant during the evolution of these rocks. If so, we expect to determine an increase in the Ta/Zr ratio with MgO depletion, which is not challenging for both series from the northern and southern parts of the Eastern Pontides. In order to determine the relative importance of the crustal contribution to the evolution of magmas from the southern and northern parts of the Eastern Pontides, a three-component mixing model using the upper Mantle (UM), the lower crust (LC) and the upper crust (UC) Sr-Nd-Pb isotopic ratios is illustrated in Fig. 13. As shown in Fig. 13, the dike samples plot on the mixing line between the upper mantle and the upper crust, and the crustal contribution to the melt of the ND and SD suites generally has a small amount, around 3%. The shift in the mixing model to the outside from the mixing line with higher $^{206}Pb/^{204}Pb$ ratio is presumably due to more radiogenic crustal contribution during subduction-related enrichment processes in the source area. Therefore, in light of all geochemical data and modelling efforts, it makes sense that AFC processes are a controlling factor for the evolution of magmas for the SD and ND suites.

5.5. Geodynamic Implications

In light of the detailed geochronological and geochemical studies, the geodynamic evolution of the Eastern Pontides was considered by many authors as a palaeo-arc setting. In recent years, even if huge numbers of data have been produced by using modern analytical techniques, the debates about the geodynamic evolution of the region have continued and a final model has not been developed yet. Although the matter of the debates mostly focus on studies about the subduction polarity, the timing of the collision and the post-collisional events, several geodynamic models were suggested such as (i) the slab breakoff model (e.g., Keskin et al. 2008; Dokuz et al. 2019), (ii) the delamination model (e.g., Altunkaynak 2007; Aydin et al. 2008; Dilek et al. 2010; Karslı et al. 2011; Arslan et al. 2013; Dokuz et al. 2013; Aydınçakır and Şen 2013; Temizel et al. 2016; Yücel et al. 2017) in a north-dipping subduction system and (iii) ridge subduction model (e.g., Eyuboglu et al. 2016, 2017) in a south-dipping subduction system. Against the contrasting beliefs about the geodynamic evolution of the Eastern Pontides, most of the researchers have reached consensus that the Eastern Pontides evolved by consecutive crustal thickening and collisional processes with an initial north-dipping subduction zone (Şengör and Yılmaz 1981; Yılmaz et al. 1997; Okay and Şahintürk 1997; Boztuğ et al. 2004). Magma generation resulted from processes damaging thermodynamic stability such as asthenospheric upwelling and decompression melting (e.g., Altunkaynak and Genç 2008; Dilek and Sandvol 2009; Dilek et al. 2010; Altunkaynak et al. 2012; Temizel et al. 2012; Arslan et al. 2013; Yücel et al. 2017). The geodynamic evolution of the Middle Eocene magmatism throughout the Eastern Pontides is best explained by the delamination model owing to data obtained during this investigation. The other models mostly fall short to explain the geodynamic evolution of the region characterised by similar volcanism in terms of geochronology, bulk-rock and isotope geochemistry with petrologic

interpretations from the northern and the southern parts of the Eastern Pontides. The slightly different age relations, isotopic budget and geochemical characteristics from both the northern and southern parts also support the delamination model as a plausible model for geodynamic evolution. The slight differences in geochronologic and petrological data such as more alkaline affinity in the northern part, increasing melting degree throughout the south and different enrichment rates in the sources may be explained by changes in the enrichment rate during initial subduction and the melting degree result of the asymmetric delamination.

In light of the present isotopic and petrochemical data, the magmas that formed Eocene volcanic rocks on both sides of the Eastern Pontides evolved from enriched mantle sources in collisional and post-collisional tectonic settings (e.g., Aydın et al., 2008; Temizel et al., 2012; Arslan et al., 2013; Aydınçakır and Şen 2013; Yücel et al., 2017). The source area of the dikes studied in both the northern and southern parts indicated that an enriched mantle source metasomatized by mostly fluid-like components during initial subduction developed beneath the region from Late Carboniferous to Early Tertiary. The metasomatism processes lead to the formation of K-rich, hydrous mineral phase-bearing net veined mantle. Prelević et al. (2008) suggested that this hydrous mineral-bearing net-veined mantle source had a lower melting degree than surrounding peridotite (Foley, 1992) existing under the entire Alpine-Himalayan orogenic system. Besides, the magmas of the studied dikes from both parts were derived from the spinel stability field according to trace element geochemistry and petrological modelling studies. The heterogeneous composition of the lithospheric mantle and the change in stress regime from compressional to extensional contributed to the evolution of mildly alkaline or calc-alkaline-alkaline transitional volcanism in the northern part and calc-alkaline-shoshonitic transitional volcanism in the southern part of the region during the Middle Eocene (Lutetian) in the post-collisional tectonic setting. Partial melting of the heterogeneous net-veined mantle in different ratios leads to formation of melt types with different affinities. The affinity of the

magmas is also affected by the melting degree. Alkaline melts are produced by melting of a vein-dominated source with low partial melting degree, while dilution of the vein melts by increased partial melting of surrounding peridotites produces shoshonitic, high-K and calc-alkaline melts (e.g., Foley 1992; Prelević et al. 2005, 2008; Conticelli et al. 2007, 2009a; Prelević et al. 2012). The generation of partial melts for Middle Eocene magmatism in the Eastern Pontides can be explained by perturbation of the geotherm subsequent to asthenospheric upwelling related to fragmented and unsymmetrical delamination (e.g., Temizel et al. 2012; Arslan et al. 2013, Temizel et al. 2016; Yücel et al. 2017) and/or slab break-off (e.g., Keskin et al. 2008; Dokuz et al. 2019) models. The E-W-, NE-SW- and NW-SE trending strike-slip movements also controlling neotectonic evolution of the Eastern Pontides contributed to the block-faulted architecture of the region and are important extensional tectonic structures in the region (Bektaş and Çapkınoğlu 1997; Maden et al. 2009). Extension related to lithospheric delamination controlled by the regional strike-slip movements in the post-collisional setting led to asthenospheric upwelling. As the delaminated fragments sink, the hot asthenosphere rises more between these fragments and comes into contact with the net-veined lithospheric mantle above. Increasing temperature with disturbed thermal equilibrium leads to an increase in melting degree and this results in melting of net-veined mantle together with surrounding peridotite. The melting of a veined mantle produces alkaline magmas including hydrous phases, whereas melting of the net-veined mantle together with surrounding peridotites leads to anhydrous mildly alkaline or alkaline-calc-alkaline transitional magmas with increasing melting degree. Fragmented and asymmetrical delamination also lead to different melting degrees in northern and southern parts. The ND suite with mildly alkaline or alkaline-calc-alkaline transitional affinity evolved by relatively low melting degree, while the H-SD group formed by melting of mostly hydrous metasomatism of net-veined mantle domains. The A-SD group evolved by melting of

peridotite-dominant mantle components with a respectively higher melting degree. Tensional fracturing of the crust under the extensional regime created pathways throughout the crust and allowed mixing processes with different levels. Based on the data from the whole rock and isotope geochemistry in addition to the petrological studies, it is obvious that the magmas of the SD and the integrated ND suites underwent FC and AFC.

6. Conclusion

Comprehensive mineral chemistry, geochronological, major, trace and rare earth elements and Sr-Nd-Pb isotope data for the basic-intermediate dikes from southern and northern parts of the Eastern Pontides allow new insights into the petrogenetic evolution of the Middle Eocene magmas and enables us to reach the following conclusions:

(1) ^{40}Ar-^{39}Ar and zircon U-Pb geochronology of the SD and ND suites reveals that the hydrous and anhydrous volcanic rocks formed in same time gap that coincided with the Middle Eocene (Lutetian).

(2) The ND suite is characterised by narrow initial $^{87}Sr/^{86}Sr$ ratios between 0.70389 and 0.70431 and εNd initial values between 1.84 and 3.75. The SD suite yielded slightly more radiogenic initial $^{87}Sr/^{86}Sr$ ratios of 0.70448 and 0.70516 with -0.17 and 1.87 indicating more enriched source composition.

(3) The source of the ND and SD suites is an enriched mantle source metasomatized by mostly fluid-like component in the spinel stability field during initial subduction-induced processes. The melting degree of the source of the magmas increased in the south and the SD suite has fingerprints of higher melting degree than the ND suite.

(4) The ND and SD suites are mostly affected by fractional crystallization and assimilation processes rather than the mixing process, according to trace element chemistry, mineral chemistry and isotope data.

(5) The parental magmas of the SD and ND suites derived from the spinel stability field and formed by melting of a net-veined mantle and surrounding peridotite source to different degrees. The magmas of the studied dikes evolved by melting of the net-veined mantle source initially metasomatized by mostly subduction-related fluids by asthenospheric upwelling due to fragmented asymmetric delamination in a post-collisional extensional tectonic environment combined with strike-slip movement at a regional scale.

Acknowledgement

This study was financially supported by Gümüşhane University Scientific Research Projects Coordination Department (GÜBAP) with the project number 16.F5118.02.01. We would like to thank Dr Frank Ramos for his support during laboratory work related to radiogenic isotope geochemistry. We are grateful to Catherine Yiğit (Skalan Gates English Language Editing and Translation Service) for professional English editing assistance. The authors also grateful to Handling Editor Orhan Karsli and Editor-in-Chief Astrid Holzheid and two anonymous reviewers for their critical and constructive comments that improved the quality of the paper.

References

Altherr R., Topuz G., Siebel W., Şen C., Meyer H.P., Satır M., Lahaye Y., 2008. Geochemical and Sr–Nd–Pb isotopic characteristics of Paleocene plagioleucitites from the eastern Pontides (NE Turkey). Lithos 105, 149–161.

Altunkaynak, Ş., 2007. Collision-driven slab breakoff magmatism in northwestern Anatolia, Turkey. The Journal of Geology 115, 63–82.

Altunkaynak, Ş., Genç, Ş.C., 2008. Petrogenesis and time-progressive evolution of the Cenozoic continental volcanism in the Biga Peninsula, NW Anatolia. Lithos, 102, 316–340, https:// doi .org /10 .1016 /j .lithos.2007 .06 .003.

Altunkaynak, Ş., Dilek, Y., Genç, C.Ş., Sunal, G., Gertisser, R., Furnes, H., Foland, K.A., Yang, J., 2012. Spatial, temporal and geochemical evolution of Oligo–Miocene granitoid magmatism in western Anatolia, Turkey. Gondwana Res. 21, 961–986.

Arslan, M., Tüysüz, N., Korkmaz, S., Kurt, H., 1997. Geochemistry and petrogenesis of the Eastern Pontide volcanic rocks, northeast Turkey. Chemie der Erde 57, 157–187.

Arslan M., Aliyazıcıoğlu İ., 2001. Geochemical and petrochemical characteristics of the Kale (Gümüşhane) volcanic rocks: implications for the Eocene evolution of Eastern Pontide arc volcanism, Northeast Turkey. Int. Geol. Rev. 43 (7), 595–610.

Arslan, M., and Aslan, Z., 2006. Mineralogy, petrography and whole-rock geochemistry of the Tertiary granitic intrusions in the Eastern Pontides, Turkey: Journal of Asian Earth Sciences 27, 177–193. doi:10.1016/j.jseaes.2005.03.002.

Arslan M., Temizel İ., Abdioğlu E., Kolaylı H., Yücel C., Boztuğ D., Şen C., 2013. ^{40}Ar-^{39}Ar dating, whole-rock and Sr-Nd-Pb isotope geochemistry of post-collisional Eocene volcanic rocks in the southern part of the Eastern Pontides (NE Turkey): implications for magma evolution in extension-induced origin. Contrib. Mineral. Petrol. 166, 113–142.

Asan, K., Kurt, H., Francis, D., Morgan, G., 2014. Petrogenesis of the Late Cretaceous K-rich rocks from the Central Pontide orogenic belt, North Turkey. Island Arc 23, 102–124.

Aslan Z., 2010. U-Pb zircon SHRIMP age, geochemical and petrographical characteristics of tuffs within calc-alkaline Eocene volcanics around Gumushane (NE Turkey), Eastern Pontides. Neues Jahr Mineral 187(3):323–346.

Aslan, Z., Arslan, M., Temizel, İ., Kaygusuz, A., 2014, K-Ar dating, whole-rock and Sr-Nd isotope geochemistry of calcalkaline volcanic rocks around the Gümüşhane area: Implications for post-collisional volcanism in the Eastern Pontides, Northeast Turkey: Mineralogy and Petrology 106, 245–267. doi:10.1007/s00710-013-0294-2.

Aydin, F., Karsli, O., Chen, B., 2008. Petrogenesis of the Neogene alkaline volcanics with implications for post-collisional lithospheric thinning of the Eastern Pontides, NE Turkey. Lithos 104, 249–266. doi:10.1016/j.lithos.2007.12.010

Aydınçakır, E., 2012. Petrography, Geochemistry and Petrogenesis of the Borçka (Artvin, NE Turkey) Area Tertiary Volcanics. Karadeniz Technical University, Trabzon (241 pp. PhD thesis).

Aydınçakır, E., Şen, C., 2013. Petrogenesis of the postcollisional volcanic rocks from the Borçka (Artvin) area: implications for the evolution of the Eocene magmatism in the Eastern Pontides (NE Turkey). Lithos 172-173, 98–117.

Aydınçakır, E., 2014. The petrogenesis of Early Eocene nonadakitic volcanism in NE Turkey: Constraints on the geodynamic implications. Lithos 208–209, 361–377. doi:10.1016/j.lithos.2014.08.019.

Aydınçakır, E., 2016. Subduction-related Late Cretaceous high K volcanism in the Central Pontides orogenic belt: Constraints on geodynamic implications. Geodinamica Acta 28, 4, 379–411. doi:10.1080/09853111.2016.1208526

Aydınçakır, E., Gündüz, R. Yücel, C., 2020. Emplacement conditions of magma(s) forming Jurassic plutonic rocks in Gümüşhane (Eastern Pontides, Turkey). Bulletin of the Mineral Research and Exploration, 162, 175-196.

Bektaş O., 1987. Volcanic belts as markers of the Mesozoic-Cenozoic active margin of Eurasia (discussion). Tectonophysics 141, 345–347.

Bektaş, O., Çapkınoğlu, Ş., 1997. Doğu Pontid magmatik arkında (KD, Türkiye) neptünyen dayklar ve blok tektoniği. Geosound 30, 451–463.

Bektaş O., Şen C., Atıcı, Y., Köprübaşı, N., 1999. Migration of the Upper Cretaceous subduction-related volcanismtoward the back-arc basin of the eastern Pontide magmatic arc (NE Turkey). Geol. J. 34, 95–106.

Blundy, J., Robinson, J., Wood, B., 1998. Heavy REE are compatible in clinopyroxene on the spinel lherzolite solidus. Earth Planet. Sci. Lett. 160, 493–504.

Boztuğ, D., Jonckheere, R., Wagner, G.A., Yeğingil, Z., 2004. Slow Senonian and fast Palaeocene-Early Eaocene uplift of the granitoids in the central eastern Pontides, Turkey: apatite fission-track results. Tectonophysics 382, 213–228.

Chorowicz, J., Dhont, D., 2002. The Black Sea: a remnant of the Paleotethyan lithosphere? EGS XXVII General Assembly (abstract # 4200).

Conticelli, S., Carlson, R.W., Widom, E., Serri, G., Beccaluva, L., Biachini, G., Wilson, M., 2007. Chemical and isotopic composition (Os, Pb, Nd, and Sr) of Neogene to Quaternary calcalkalic, shoshonitic and ultrapotassic mafic rocks from the Italian peninsula: inferences on the nature of their mantle sources. Cenozoic Volcanism in the Mediterranean Area. Geological Society of America, Special Papers 418, pp. 171–202.

Conticelli, S., Marchionni, S., Rosa, D., Giordano, G., Boari, E., Avanzinelli, R., 2009a. Shoshonite and sub-alkaline magmas from an ultrapotassic volcano: Sr-Nd-Pb isotope data on the Roccamonfina volcanic rocks, Roman Magmatic Province, Southern Italy. Contrib. Mineral. Petrol. 157, 41–63.

Çamur, M.Z., Güven, İ.H., Er, M., 1996. Geochemical characteristics of the eastern Pontide volcanics: An example of multiple volcanics cycles in arc evolution. Turkish Journal of Earth Sciences 5, 123–144.

Çapkınoğlu, Ş., 2003. First records of conodonts from the Permo-Carboniferous of Demirözü (Bayburt), Eastern Pontides, NE Turkey. Turkish Journal of Earth Sciences 12, 199–217.

Deer WA, Howie RA, Zussman J., 1992. An Introduction to the rock forming minerals, 2nd edn. Longman, London, 696 pp.

Dilek, Y., Sandvol, E., 2009. Seismic structure, crustal architecture and tectonic evolution of the Anatolian-African Plate Boundary and the Cenozoic Orogenic Belts in the Eastern Mediterranean Region. In: Murphy, J.B., Keppie, J.D., Hynes, A.J. (Eds.), Ancient Orogens and Modern Analogues. Geological Society of London, Special Publications 327, pp. 127–160.

Dilek, Y., Imamverdiyev, N., Altunkaynak, Ş., 2010. Geochemistry and tectonics of Cenozoic volcanism in the Lesser Caucasus (Azerbaijan) and the Iberi-Arabian region: Collision-induced mantle dynamics and its magmatic fingerprint. International Geology Review 52, 4-6, 536–578, https:// doi .org /10 .1080/00206810903360422 .

Dokuz, A., 2011. A slab detachment and delamination model for the generation of Carboniferous high-potassium I type magmatism in the Eastern Pontides, NE Turkey: the Köse composite pluton. Gondwana Res. 19:926–944.

Dokuz, A., Tanyolu, E., 2006. Geochemical constraints on the provenance, mineral sorting and subaerial weathering of lower Jurassic and Upper Cretaceous clastic rocks from the Eastern Pontides, Yusufeli (Artvin), NE Turkey. Turkish Journal of Earth Sciences 15, 181–209.

Dokuz, A., Karslı, O., Chen, B., Uysal, İ., 2010. Sources and petrogenesis of Jurassic granitoids in the Yusufeli area, northeastern Turkey: implications for pre- and post-collisional lithospheric thinning of the Eastern Pontides. Tectonophysics 480:259–279.

Dokuz, A., Uysal, İ., Siebel, W., Turan, M., Duncan, R., Akçay, M., 2013. Post-collisional adakitic volcanism in the eastern part of the Sakarya Zone, Turkey: Evidence for slab and crustal melting. Contributions to Mineralogy and Petrology 166, 1443–1468. doi:10.1007/s00410-0130936-8.

Dokuz, A., Uysal, İ., Dilek, Y., Karslı, O., Meisel, T., Kandemir, R., 2015. Geochemistry, Re-Os isotopes and highly siderophile element abundances in the Eastern Pontide peridotites (NE Turkey): Multiple episodes of melt extraction-depletion, melt-rock interaction and fertilization of the Rheic Ocean mantle: Gondwana Research 27, 612–628.

Dokuz, A., Aydınçakır, E., Kandemir, R., Karslı, O., Siebel, W., Derman, A.S., Turan, M., 2017. Late jurassic magmatism and stratigraphy in the Eastern Sakarya zone, Turkey: Evidence for the slab breakoff of paleotethyan oceanic lithosphere. The Journal of Geology 125, 1–3. doi:10.1086/689552.

Dokuz A., Aydin F., Karslı O., 2019. Postcollisional transition from subduction- to intraplate type magmatism in the eastern Sakarya zone, Turkey: Indicators of northern Neotethyan slab breakoff. The Geological Society of Amerika. (in press). doi.org/10.1130/B31993.1

Duncan, A. R., Erlank, A. J., Marsh, J. S. 1984. Regional geochemistry of the Karoo igneous province. In: Erlank, A. J. (ed.) Petrogenesis of the Volcanic Rocks of the Karoo Province. Special Publication of the Geological Society of South Africa 13, 355-388.

Ekici, T., 2016. Petrology and Ar/Ar choronology of Erdembaba and Kuyucak volcanics exposed along the North Anatolian fault zone (Eastern Pontides, NE Turkey): Implications for the late cenozoic geodynamic evolution of Eastern Mediterranean Region. Journal Geology Society of India 87, 1–13.

M.A. Elburg, M. van Bergen, J. Hoogewerff, J. Foden, P. Vroon, I. Zulkarnain, A., 2002. Nasution Geochemical trends across an arc-continent collision zone: magma sources and slab-wedge transfer processes below the Pantar Strait volcanoes. Indonesia Geochim. Cosmochim. Acta 66 2771-2789.

Eyüboğlu, Y., Bektaş, O., Seren, A., Maden, N., Jacoby, W.R., Özer, R., 2006. Three axial extensional deformation and formation of the Liassic rift basins in the Eastern Pontides (NE Turkey). Geologica Carpathatica 57, 5, 337–346.

Eyuboglu, Y., 2010. Late Cretaceous high-K volcanism in the eastern Pontide orogenic belt: Implications for the geodynamic evolution of NE Turkey. International Geology Review 52(2–3), 142–186.

Eyuboglu, Y., Santosh, M., Chung, S.-L., 2011. Petrochemistry and U-Pb Zircon Ages of Adakitic Intrusions from the Pulur Massif (Eastern Pontides, NE Turkey): Implications for Slab Rollback and Ridge Subduction Associated with Cenozoic Convergent Tectonics in the Eastern Mediterranean. The Journal of Geology 119, 394–417. doi:10.1086/660158

Eyuboglu Y., Santosh M., Yi, K., Bektaş O., Kwon S., 2012a. Discovery of Miocene adakitic dacite from the Eastern Pontides Belt and revised geodynamic model for the late Cenozoic Evolution of eastern Mediterranean region. Lithos 146–147, 218–232.

Eyuboglu, Y., Santosh, M., Dudas, F.O., Akaryali, E., Chung, S.L., Akdag, K., Bektas, O., 2013. The nature of transition from adakitic to non-adakitic magmatism in a slab-

window setting: a synthesis from the eastern Pontides, NE Turkey. Geoscience Frontiers 4, 353–375.

Eyuboglu, Y., Dudas, F.O., Santosh, M., Zhu, D.C., Yi, K., Chatterjee, N., Akaryali, E., Liu, Z., 2016. Cenozoic forearc gabbros from the northern zone of the Eastern Pontides Orogenic Belt, NE Turkey: implications for slab window magmatism and convergent margin tectonics. Gondwana Research 33, 160–190.

Eyuboglu Y., Dudas F.O., Thorkelson D., Zhu D., Liu Z., Chatterjee N., Yi K., Santosh M., 2017. Eocene granitoids of northern Turkey: Polybaric magmatism in an evolving arc–slab window system. Gondwana Research, 50, 311–345.

Ewart, A., 1982. The mineralogy and petrology of TertiaryRecent orogenic volcanic rocks: With special reference to the andesitic-basaltic compositional range. in Thorpe, R.S., ed., Andesites: Chichester, J. Wiley and Sons, p. 25- 95.

Ewart, A., Marsh, J. S., Milner, S. C., Duncan, A. R., Kamber, B. S., Armstrong, R. A. 2004. Petrology and geochemistry of Early Cretaceous bimodal continental flood volcanism of the NW Etendeka, Namibia. Part 1: Introduction, mafic lavas and re-evaluation of mantle source components. Journal of Petrology 45, 59-105.

Foley, S., 1992. Vein-plus-wall-rock melting mechanisms in the lithosphere and the origin of potassic alkaline magmas. Lithos 28, 435–453.

Frey, F.A., Green, D.H., Roy, S.D., 1978. Integrated models of basalt petrogenesis: a study of quartz tholeiites to olivine melilites fromSouth Eastern Australia utilizing geochemical and experimental petrological data. J. Petrol. 19, 463–513.

Furman, T., Graham, D., 1999. Erosion of lithospheric mantle beneath the East African Rift system: Geochemical evidence from the Kivu volcanic province. Lithos 48, 237–262. doi:10.1016/S0024-4937(99)00031-6.

Gehrels, G.E., Valencia, V.A., Ruiz, J., 2008. Enhanced precision, accuracy, efficiency, and spatial resolution of U-Pb ages by laser ablation–multi collector–inductively coupled plasma–mass spectrometry. Geochemistry Geophysics Geosystems, Q03017, doi: 10.1029/2007GC001805.

Genç S. C., Yilmaz, Y., 1995. Evolution of the Triassic continental margin, Nortwest Anatolia. Tectonophysics 243, 193–207.

Genç, S. C., Gulmez, F., Karacık, Z., Tuysuz, O., Prelevic, D., Roden, M. F., Billor, M. Z., 2014. Subduction-related High-to Ultrahigh-Potassic Rocks of the Ankara-Erzincan Suture Belt of Turkey: A geochemical and isotopic approach to source and petrogenesis. Geophysical Research Abstracts. 16, 365 pp., EGU General Assembly.

Guo, Z., J. Hertogen, J. Liu, P. Pasteels, A. Boven, L. Punzalan, H. He, X. Luo, W. Zhang., 2005. Potassic magmatism in western Sichun and Yunnan provinces, SE Tibet, China: petrological and geochemical constraints on petrogenesis. J. Petrol. 46 33-78.

Gülmez, F., Genç, C., 2015. Differentiation processes in Late Cretaceous ultrapotassic volcanics around Amasya. Bulletin of the Mineral Research and Exploration 151, 149–168.

Gülmez F., Genç Ş.C., Prelevic D., Tüysüz O., Karacık Z., Roden M.F., Billor Z., 2017. Ultrapotassic Volcanism from the Waning Stage of the Neotethyan Subduction: a Key Study from the Izmir–Ankara–Erzincan Suture Belt, Central Northern Turkey. Journal of Petrology 57 (3), 561-593.

Hanes, J.A., York, D., Hall, C.M., 1985. An $^{40}Ar/^{39}Ar$ geochronological and electron microprobeinvestigation of an Archean pyroxenite and its bearing on ancient atmospheric compositions. Can. J. Earth Sci. 22, 947-958.

Hart, S.R. Davis, K.E., 1978. Nickel partitioning between olivine and silicate melt. Earth and Planetary Science Letters 40 203-219. doi: 10.1016/0012-821X(78)90091-2.

Hawkesworth, C.J., Turner, S.P., Peate, D.W., McDermott, F., van Calsteren, P., 1997. U-Th isotopes in arc magmas: implications for element transfer from the subducted crust. Science 276, 551–555.

Ionov, D.A., Griffin, W.L., O'Reilly, S.Y., 1997. Volatile bearing minerals and lithophile trace elements in the upper mantle. Chemical Geology 141, 153–184. doi:10.1016/S0009-2541(97)00061-2.

Irvine, T.N., Baragar, W.R.A., 1971. A guide to the chemical classification of the common volcanic rocks. Canadian Journal of Earth Sciences 8, 5, 523–548. doi:10.1139/e71-055

Kandemir, R., 2004. Gümüşhane yakın yörelerindeki Erken-Orta Jura Yaşlı Şenköy Formasyonu'nun Çökel Özellikleri ve Birikim Koşulları. PhD thesis, Karadeniz Teknik Üniversitesi Fen Bilimleri Enstitüsü (In Turkish with English abstract).

Kandemir, R., Yılmaz, C., 2009. Lithostratigraphy, facies, and deposition environment of the lower Jurassic Ammonitico Rosso type sediments (ARTS) in the Gümüşhane, area, NE Turkey: implications for the opening of the northern branch of the NeoTethys Ocean. Journal of Asian Earth Sciences 34, 586–598.

Kandemir, R., Lerosey-Aubril, R., 2011. First report a trilobite in the Carboniferous of Eastern Pontides, NE Turkey. Turkish Journal of Earth Sciences 20, 179–183.

Karsli, O., Chen, B., Uysal, İ., Aydin, F., R. Wijbrans, J., Kandemir, R., 2008. Elemental and Sr–Nd–Pb isotopic geochemistry of the most recent Quaternary volcanism in the

Erzincan Basin, Eastern Turkey: framework for the evaluation of basalt–lower crust interaction. Lithos 106, 55-70.

Karslı, O., Dokuz, A., Uysal, İ., Aydın, F., Kandemir, R., Wijbrans, J., 2010. Generation of the early Cenozoic adakitic volcanism by partial melting of mafic lower crust, eastern Turkey: implications for crustal thickening to delamination. Lithos 114:109–120.

Karslı, O., Uysal, İ., Ketenci, M., Dokuz, A., Aydin, F., Kandemir, R., Wijbrans, J., 2011. Adakite-like granitoid porphyries in Eastern Pontides, NE Turkey: Potential parental melts and geodynamic implications. Lithos 127, 354–372, https:// doi .org /10 .1016 /j.lithos .2011 .08 .014 .

Karslı, O., Dokuz, A., Kaliwoda, M., Uysal, İ., Aydın, F., Kandemir, R., Fehr, K. T., 2014. Geochemical fingerprints of Late Triassic calc-alkaline lamprophyres from the Eastern Pontides, NE Turkey: a key to understanding lamprophyre formation in a subduction related environment. Lithos 196, 181–197.

Karslı O., Aydin F., Uysal İ., Dokuz, A, Kumral, M, Kandemir R., Budakoğlu M., Ketenci M., 2018. Latest Cretaceous "A2-type" granites in the Sakarya zone, NE Turkey: Partial melting of mafic lower crust in response to roll-back of Neo-Tethyan oceanic lithosphere. Lithos 302–303, 312–328.

Kaygusuz, A., Aydinçakir, E., 2011. Petrogenesis of a Late Cretaceous composite pluton from the eastern Pontides: The Dağbaşı pluton, NE Turkey. Neues Jahrbuch Für Mineralogie - Abhandlungen 188, 3, 211–223. doi:10.1127/0077-7757/2011/0201.

Kaygusuz, A., Aslan Z., Siebel, W., Sen, C., 2011. Geochemical and Sr–Nd isotopic characteristics of post-collisional calc-alkaline volcanics in the Eastern Pontides (NE Turkey). Turkish J Earth Sci 20,137–159.

Kaygusuz, A., Arslan, M., Siebel, W., Sipahi, F., Ilbeyli, N., 2012. Geochronological evidence and tectonic significance of Carboniferous magmatism in the southwest Trabzon area, Eastern Pontides, Turkey. Int. Geol. Rev. 54, 1776–1800.

Kaygusuz, A., Öztürk, M., 2015. Geochronology, geochemistry, and petrogenesis of the Eocene Bayburt intrusions, Eastern Pontides, NE Turkey: Evidence for lithospheric mantle and lower crustal sources in the high-K calc-alkaline magmatism. Journal of Asian Earth Sciences 108, 97–116. doi:10.1016/j.jseaes.2015.04.017

Kaygusuz, A., Arslan, M., Sipahi, F., and Temizel, İ., 2016. U-Pbzircon chronology and petrogenesis of Carboniferous plutons in the northern part of the Eastern Pontides, NE Turkey: Constraints for Paleozoic magmatism and geodynamic evolution. Gondwana Research 39, 327–346. doi:10.1016/j.gr.2016.01.011.

Kaygusuz, A., Şahin, K., 2016. Petrochemical, geochemical and petrological characteristics of Eocene volcanic rocks in the Mescitli area, Eastern Potides (NE Turkey). Journal of Engineering Research and Applied Science 5, 2, 473–486.

Kaygusuz A., Yücel C., Arslan M., Temizel İ., Yi K., Jeong Y.J., Seibel W., Sipahi F., 2020. Eocene I-type magmatism in the Eastern Pontides, NE Turkey: insights into magma genesis and magma-tectonic evolution from whole-rock geochemistry, geochronology and isotope systematics. International Geology Review 62, 11, 1406–1432

Keskin, M., Genç, S.C., Tüysüz, O., 2008. Petrology and geochemistry of post-collisional Middle Eocene volcanic units in North-Central Turkey: evidence for magma generation by slab breakoff following the closure of the Northern Neotethys Ocean. Lithos 104, 267–305.

Klemme, S., 2004. The Influence of Cr on the Garnet-Spinel Transition in the Earth's Mantle: Experiments in the System MgO-Cr2O3-SiO2 and Thermodynamic Modeling. Lithos 77, 639–646.

Le Bas, M. J., Le Maitre, R.W., Streckeisen, A. Zanettin, B., 1986. A chemical classification of volcanic rocks based on the total alkali-silica diagram. Journal of Petrology 27, 745-750.

Ludwig K.R., 2008. Isoplot 3.6, Berkeley Geochronology Center Spec. Pub. No. 4, 77 pp.

Maden, N., Gelişli, K., Eyüboğlu, Y., Bektaş, O., 2009. Two-and-three-dimensional crustal thickness of the eastern Pontides (NE Turkey). Turk. J. Earth Sci. 18 (2), 225–238.

McKenzie, D.P., O'Nions, R.K., 1991. Partial melt distributions from inversion of rare earth element concentrations. Journal of Petrology 32, 1027–1091.

Nielsen, C. H., Sigurdsson H., 1981. Quantitative methods for electron microprobe analysis of sodium in natural and synthetic glasses. American Mineralogist 66, 547–552.

Nikishin, A.M., Okay, A.I., Tüysüz, O., Demirer, A., Wannier, M., Amelin, N., Petrov, E. 2015. The Black Sea basins structure and history: New model based on new deep penetration regional seismic data. Part 2: Tectonic history and paleogeography. Marine and Petroleum Geology 59, 656-670.

Okay, A.İ., Şahintürk, O., 1997. Geology of the eastern Pontides, in Robinson, A.G., ed., Regional and petroleumgeology of the Black Sea and surrounding region: Tulsa, Oklahoma. American Association of Petroleum Geologists 68, 291–311.

Pearce, J.A., Bender, J.F., De Long, S.E., Kidd, W.S.F., Low, P.J., Güner, Y., Saroglu, F., Yilmaz, Y., Moorbath, S., Mitchell, J.G., 1990. Genesis of collision volcanism in

eastern Anatolia Turkey. Journal of Volcanology and Geothermal Research 44, 189–229. doi:10.1016/0377-0273(90)90018-B.

Pelin, S., 1977. Alucra (Giresun) Güneydoğu Yöresinin Petrol Olanakları Bakımından İncelenmesi, PhD Thesis. Karadeniz Teknik Üniversitesi Yer Bilimleri Fakültesi, No. 13, Trabzon, 115 p. (in Turkish).

Prelević, D., Foley, S.F., Romer, R.L., Cvetković, V., Downes, H., 2005. Tertiary ultrapotassic volcanism in Serbia: constraints on petrogenesis and mantle source characteristics. J. Petrol. 46, 1443–1487.

Prelević, D., Foley, S.F., Romer, R.L., Conticelli, S., 2008. Mediterranean Tertiary lamproites derived from multiple source components in postcollisional geodynamics. Geochim. Cosmochim. Acta 72, 2125–2156.

Prelević, D., Akal, C., Foley, S.F., Romer, R.L., Strack[illegible] A., Van Den Bogaard, P., 2012. Ultrapotassic mafic rocks as geochemical proxies for post-collisional dynamics of orogenic lithospheric mantle: the case of southwestern Anatolia, Turkey. J. Petrol. 53, 1019–1055.

Ramos, F.C., 1992. Isotope Geology of Metamorphic Core of the Central Grouse Creek Mountains, Box Elder Country, Utah (MSc thesis), University of California, Los Angeles.

Renne, P.R., Swisher, C.C., Deino, A.L., Karner, D.B., Owens, T.L., DePaolo, D.L., 1998. Intercalibration of standards, absolute ages and uncertainties in $^{40}Ar/^{39}Ar$ dating. Chem.Geol. 145, 117–152.

Renne, P.R., Mundil, R., Balco, G., Min, K., Ludwig, K.R., 2010. Joint determination of 40K decay constants and $^{40}Ar^{*}/^{40}K$ for the Fish Canyon sanidine standard, and improved accuracy for $^{40}Ar/^{39}Ar$ geochronology. Geochim. Cosmochim. Acta 74, 5349–5367.

Renne, P.R., Balco, G., Ludwig, K.R., Mundil, R., Min, K., 2011. Response to the comment by W.H. Schwarz et al. on "Joint determination of ^{40}K decay constants and K for the Fish Canyon sanidine standard, and improved accuracy for $^{40}Ar/^{39}Ar$ geochronology" by P.R. Renne et al., 2010. Geochim. Cosmochim. Acta 75, 5097–5100.

Robinson, J. A. C., Wood, B. J., 1998. The Depth of the Garnet/Spinel Transition in Fractionally Melting Peridotite. Earth and Planetary Science Letters, 164, 277–284

Roddick, J.C., Cliff, R.A., Rex, D.C., 1980. The evolution of excess argon in alpine biotites – a ^{40}Ar-^{39}Ar analysis. Earth Planet. Sci. Lett. 48, 185–208.

Ruffet G., Féraud G., Amouric M., 1991. Comparison of $^{40}Ar/^{39}Ar$ conventional and laser dating of biotites from the North Trégor Batholith. Geochim. Cosmochim. Acta 55, 1675–1688.

Ruffet, G., Féraud, G., Ballèvre, M., Kiénast, J.R., 1995. Plateau ages and excess argon in phengites: an $^{40}Ar–^{39}Ar$ laser probe study of Alpine micas (Sesia Zone, Western Alps, northern Italy). Chemical Geology (Isotopic Geoscience Section) 121, 327–343.

Sengör, A.M.C., Yilmaz, Y., 1981. Tethyan evolution of Turkey: A plate tectonic approach: Tectonophysics 75, 181–241. doi:10.1016/0040-1951(81)90275-4.

Shaw, D.M., 1970. Trace element fractionation during anatexis. Geochim. Cosmochim. Acta 34, 237–259.

Shaw, J.E., Baker, J.A., Menzies, M.A., Thirlwall, M.F., Ibrahim, K.M., 2003. Petrogenesis of the largest intraplate volcanic field on the Arabian plate (Jordan): a mixing lithosphere-asthenosphere source activated by lithospheric extension. J Petrol 44,1657–1679.

Taylor, S.R., Mclennan, S.M., 1985. The continental crust: Its composition and evolution: Oxford, Blackwell, Scientific Publication 312 p.

Temizel, I., Arslan, M., 2009. Mineral chemistry and petrochemistry of post-collisional Tertiary mafic to felsic cogenetic volcanics in the Ulubey (Ordu) area, eastern Pontides, NE Turkey. Turkish J Earth Sci 18, 29–53.

Temizel, I., Arslan, M., Ruffet, G., Peucat, J.J. 2012. Petrochemistry, geochronology and Sr–Nd isotopic systematics of the Tertiary collisional and post-collisional volcanic rocks from the Ulubey (Ordu) area, eastern Pontide, NE Turkey: implications for extension-related origin and mantle source characteristics. Lithos 128, 126–147.

Temizel, İ., Arslan, M., Yücel, C., Abdioğlu, E., Ruffet, G., 2016. Geochronology and geochemistry of Eocene-aged volcanic rocks around the Bafra (Samsun, N Turkey) area: constraints for the interaction of lithospheric mantle and crustal melts. Lithos 258-259, 92–114.

Temizel, İ., Arslan, M., Yücel, C., Yazar, E.A., Kaygusuz, A., Aslan, Z. 2019. U-Pb geochronology, bulk-rock geochemistry and petrology of Late Cretaceous syenitic plutons in the Gölköy (Ordu) area (NE Turkey): Implications for magma generation in a continental arc extension triggered by slab roll-back. Journal of Asian Earth Sciences 171, 305-320.

Thirlwall, M.F., Smith, T.E., Graham, A.M., Theodorou, N., Hollings, P., Davidson, J.P., Arculus, R.J., 1994. High field strength element anomalies in arc lavas; source or process? J Petrol 35, 819–838.

Topuz, G., Altherr, R., Schwarz, W. H., Siebel, W., Satır, M., Dokuz, A., 2005. Post-collisional plutonism with adakite-like signatures: The Eocene Saraycık granodiorite (Eastern Pontides, Turkey). Contributions to Mineralogy and Petrology 150, 441–455.

Topuz, G., Altherr, R., Schwarz, W.H., Dokuz, A., Meyer, H.-P., 2007. Variscan amphibolite-facies rocks from the Kurtoğlu metamorphic complex (Gümüşhane area, Eastern Pontides, Turkey). International Journal of Earth Sciences 96, 861–873. doi:10.1007/s00531-006-0138-y.

Topuz, G., Altherr, R., Siebel, W., Schwarz, W.H., Zack, T., Hasözbek, A., Barth, M., Satır, M., and Şen, C., 2010. Carboniferous high-potassium I-type granitoid magmatism in the Eastern Pontides: The Gümüşhane pluton (NE Turkey) Lithos 116, 92–110. doi:10.1016/j. lithos.2010.01.003.

Turner, G., 1971. ^{40}Ar-^{39}Ar ages from the lunar Maria. Earth Planet. Sci. Lett. 11, 169–191.

Turner, S.P., 2002. On the time-scales of magmatism at island-arc volcanoes. Philos. Trans. R. Soc. Lond. Ser. A 360, 2853–2871.

Turner, S., Arnaud, N., Liu, J., Rogers, N., Hawkesworth, C., Harris, N., Kelley, S., van Calsteren, P., Deng, W., 1996. Post-collision, shoshonitic volcanism on the Tibetan Plateau: implications for convective thinning of the lithosphere and the source of ocean island basalts. Journal of Petrology 37, 45-71.

Turner S., Hawkesworth C., Rogers N., Bartlett J., Worthington T., Hergt, J., Pearce J., Smith I., 1997. ^{238}U–^{230}Th disequilibria, magma petrogenesis, and flux rates beneath the depleted Tonga-Kermadec island arc Geochim. Cosmochim. Acta, 61, 4855-4884.

Yang, W., Niu, H., Shan, Q., Luo, Y., Sun, W., Li, C., Li, N., Yu, X., 2012. Late Paleozoic calcalkaline to shoshonitic magmatism and its geodynamic implications, Yuximolegai area, western Tianshan, Xinjiang. Gondwana Res. 22, 325–340.

Yılmaz, C., Korkmaz, S., 1999. Basin development in the Eastern Pontides, Jurassic to Cretaceous, NE Turkey: Zentralblatt für Geologie und Palaontologie, Teil I, 10–12, 1485–1494.

Yılmaz, Y., Tüysüz, O., Yiğitbaş, E., Genç, Ş.C., Şengör, A.M.C., 1997. Geology and tectonic evolution of the Pontides, in Robinson, A.G., ed., Regional and petroleum geology of the Black Sea and surrounding region: Tulsa, Oklahoma, American Association of Petroleum Geologists, 68, 183–226.

Yücel C., Arslan M., Temizel İ., Abdioğlu E., 2014a. Volcanic facies and mineral chemistry of Tertiary volcanics in the northern part of the Eastern Pontides, northeast Turkey: implications for pre-eruptive crystallization conditions and magma chamber processes. Mineral. Petrol. 108-3, 439–467.

Yücel, C., Temizel, İ,Abdioğlu, E., Arslan, M., Yağcıoğlu, U.C., 2014b. Origin of analcimes in the Tertiary volcanic rocks from the Eastern Pontides (NE Turkey): a textural, mineralogical and geochemical approach. J. Mineral. Geochem 191 (3), 277–299.

Yücel C., 2017. Akçaabat (Trabzon) Güneyi ve Çevresindeki Kampaniyen Yaşlı Volkanik Kayaçların Petrografisi, Jeokimyası, Jeokronolojisi ve Petrojenezi. GÜFBED/GUSTIJ, 7 (1): 79-101

Yücel C., Arslan M., Temizel İ., Abdioğlu E., Ruffet G., 2017. Evolution of K-rich magmas derived from a net veined lithospheric mantle in an ongoing extensional setting: Geochronology and geochemistry of Eocene and Miocene volcanic rocks from Eastern Pontides (Turkey) Gondwana Research 45, 65–85. doi:10.1016/j.gr.2016.12.016.

Yücel C., 2019. Geochronology, geochemistry, and petrology of adakitic Pliocene–Quaternary volcanism in the Şebinkarahisar (Giresun) area, NE Turkey. Int. Geo. Rev. 61(6), 754-777.

Figure Captions

Figure 1. (a) The tectonic units and the main suture zones of Turkey (after Okay and Tüysüz 1999); (b) the simplified geological map of the Eastern Pontides showing distribution of the Eocene and Miocene–Quaternary volcanic rocks. Modified after Güven (1993), Arslan et al. (2013) and Temizel (2014).

Figure 2. (a) The simplified geological map of the Yeniyol-Kale (Gümüşhane) area, and (b) the study area, showing the orientation of the basic-intermediate dikes and the sample locations (Modified after Karslı et al 2010; Eyuboglu et al. 2013).

Figure 3. Representative microphotographs of the basic-intermediate samples; (a,b) clinopyroxene, plagioclase and opaque phenocrysts in microlithic porphyritic texture, (c) plagioclase and clinopyroxene with opaque mineral accumulation, (d) plagioclase and clinopyroxene with opaque inclusion, (e,f) hornblende, plagioclase and opaque phenocrysts in microlithic porphyritic and fluidal textures, respectively.

Figure 4. (a) Concordia plots showing the U–Pb analyses of the zircons, (b) average age plot for the SD suite, (c, e) ^{40}Ar-^{39}Ar Age spectra and plateau and (d, f) inverse isochrones ages acquired by step heating of whole-rock for the SD suite.

Figure 5. Chemical classification and nomenclature plots for the studied SD suite in the Gümüşhane area, compared with ND suite in the Trabzon area (Yücel et al 2017), using (a) the total alkalis versus silica (TAS) diagram (after Le Bas et al., 1986) (the alkaline and subalkaline discrimination line after Irvine and Baragar, 1971), (b) Zr/TiO_2*0.0001 versus Nb/Y diagram (after Winchester and Floyd, 1976),(c) SiO_2 versus K_2O plot (after Ewart, 1982), (d) AFM diagram of Irvine and Baragar (1971).

Figure 6. SiO_2(wt%) versus major oxide (wt%), trace element (ppm) variation plots of the studied SD suite (symbols are as in Fig. 5).

Figure 7. (a) Primitive mantle-normalized (Sun and Mcdonough 1989) spider plots and (b) chondrite (Taylor and Mclennan 1985) normalized rare earth element plots of the studied SD suite, compared with ND suite (Yücel et al 2017) (symbols are as in Fig. 5). OIB and N-MORB compositions from Winter (2001).

Figure 8. (a) $(^{143}Nd/^{144}Nd)_i$ versus $(^{87}Sr/^{86}Sr)_i$ plot showing the studied SD suite and ND suite (Yücel et al 2017). For the comparison, the samples from other alkaline and calcalkaline volcanic rocks of the region were plotted as Borçka volcanic rocks (Aydınçakır and Şen, 2013), Torul volcanic rocks (Kaygusuz et al., 2011), the southern part Eocene volcanic rocks (Arslan et al., 2013), Everek Hanları volcanic rocks (Altherr et al., 2008; Eyüboğlu, 2010), Ulubey volcanic rocks (Temizel et al., 2012), Kop Adakites (Eyüboğlu et al., 2013), Kale Adakites (Karslı et al., 2010). Data for lithospheric mantle array from Davies and von Blanckenburg (1995). Compositions of MORB (mid-ocean ridge basalt) and mantle array from Wilson (1989), Gill (1981) and McCulloch et al. (1994); EMI (enriched mantle type I)

and EMII (enriched mantle type II), HIMU (high μυ: mantle with high U/Th ratio), DM (Depleted Mantle) fields and CHUR (Chondritic Uniform Reservoir)-Sr and -Nd reference lines after Zindler and Hart (1986). (b, c) variations in Pb isotope compositions of the samples from Eocene aged Trabzon and Gümüşhane volcanic rocks. Plotted for comparison, the composition of pelagic sediments and MORB are after Peate et al. (1997) and Hofmann (2003), NHRL (Northern Hemisphere Reference Line) after Hart (1984), EAR (Depleted East European Lithosphere) after Rosenbaum et al. (1997), North African sediments after Pe- Piper (1994), DM (depleted mantle), HIMU and enriched (EMI and EMII) mantle after Zindler and Hart (1986). Field of arc systems (compiled in Wilson (1989) and Winter (2001) (symbols are as in Fig. 5).

Figure 9. (a) Plot of Sm/Yb versus Sm, (b) Dy/Yb versus La/Yb and (c) Rb/Sr versus Ba/Rb plot for the studied SD suite and the ND suite (Yücel et al 2017). Non-modal batch melting curves were calculated by using partition coefficients from Robinson (1993), McKenzie and O'Nions (1991) and Keskin (2002) (symbols are as in Fig. 5).

Figure 10. (a) Th/Yb versus Ta/Yb plot (after Pearce, 1983). Average N-MORB composition and average Continental Crust (Av. CC) compositions are from Sun and McDonough (1989) and Taylor and McLennan (1985), respectively. Vectors reflecting inferred effects of fractional crystallisation (FC), assimilation-fractional crystallisation (AFC), subduction enrichment and mantle metasomatism are from Pearce et al.1990). (b) the plot of Ba/Th versus Th, (c) Th/Yb versus Ba/La diagram, the shaded area indicates the oceanic arc volcanic rocks (Kirchenbaur et al. (2012) and references therein). (d) Sr/La versus La/Yb, (e) Th/La versus Ce/Pb plots for the studied SD suite and the ND suite (Yücel et al 2017) (symbols are as in Fig. 5).

Figure 11. (a, b, c) K/Rb versus Rb, Ba versus Sr and Sr versus MgO (wt.%) plots indicating the major fractionating phases, (d) Co versus Th plot, displaying theoretical Rayleigh fractionation lines (curve 1, cpx_{50} pl_{50}; curve 2, ol_{25} cpx_{25} pl_{50}; curve 3, cpx_5 pl_{60} hbl_{25} bi_5 mg_5; curve 4, cpx_{20} pl_{30} hbl_{45} mg_5; curve 5, cpx_{35} pl_{50} hbl_{15}). The FC modeller program of Keskin (2002) was used to calculate the plot of curves (symbols are as in Fig. 5).

Figure 12. (a) $(^{87}Sr/^{86}Sr)_i$ versus SiO_2, (b) $(^{143}Nd/^{144}Nd)_i$ versus SiO_2 plots showing possible fractional crystallisation (FC) and/or assimilation-fractional crystallisation (AFC) trends, (c) $(Th/Yb)_{PM}$ versus $(Nb/Yb)_{PM}$ and (d) MgO versus Ta/Zr diagrams for the studied SD suite and the ND suite (Yücel et al 2017) (symbols are as in Fig. 5).

Figure 13. (a) εNd versus $^{87}Sr/^{86}Sr$, (b) εNd versus $^{206}Pb/^{204}Pb$ and (c) $^{87}Sr/^{86}Sr$ versus $^{206}Pb/^{204}Pb$ plots showing a three-component mixing model between upper/lower crust and upper mantle for the studied SD suite and the ND suite (Yücel et al 2017). Tick marks on mixing lines are at 10% intervals. (symbols are as in Fig. 5).

Table Captions

Table 1. Generalized mineralogy and textural features of the Eocene-aged SD suite.

Table 2. Whole-rock major oxide (wt%) trace and rare earth element (ppm) analyses from Eocene-aged SD suite.

Table 3. Sr and Nd isotopic analysis of Eocene aged SD suite from the Trabzon and Gümüşhane areas.

Table 4. Partition coefficient (D). normative weight fractions of minerals and source modal composition data used in partial melting modelling calculation.

Table 5. Compiled Kd values used in fractional crystallization (FC) modelling calculation.

Table 6. The compositions assumed for the end member (UP: upper mantle. UC: upper crust. LC: lower crust) components of Sr–Nd–Pb isotopic mixing model.

Tables

Table 1.

		Sample	Pl	Cpx	Ol	Hbl	Sa	Opq	Common Textures
The SPD series	The A-SPD group	B-7	+	+	?			+	
		B-13	+	+				+	
		B-20	+	+	+			+	
		B-23	+	+				+	microlitic porphyritic
		B-24	+	+				+	hyalo-microlitic porphyritic. glomeroporphyritic
		B-42	+	+				+	
		B-44	+	+				+	
		B-45	+	+				+	
	The H-SPD group	B-26	+			+	?	+	
		B-30	+			+	?	+	flow
		B-31	+			+	?	+	microlo[illegible]c p[illegible]rphyritic glomeroporphyritic
		B-32	+			+	?	+	poikilitic
		B-37	+			+	?	+	

Pl, plagioclase; Cpx, clinopyroxene; Ol, olivine; Hbl, hornblende; Sa, sanidine; Op, opaque mineral

Table 2.

Sample	H-SPD					A-SPD										
No	B26	B30	B37	B32	B31	B2	B7	B13	B20	B24	B23	B42	B45	B44	B48	B46
Coordinates	37T 556866E 4473339N	37T 556084E 4473787N	37T 555752E 4474257N	37T 556084E 4473787N	37T 556084E 4473787N	37T 552600E 4473594N	37T552550E 4473580N	37T 552500E 4473530N	37T 556194E 4473735N	37T 556194E 4473735N	37T 556080E 447363[illegible]N	37T 556325E 4473480N	37T 557025E 4473480N	37T 556531E 4473392N	37T 556531E 4473392N	37T 556531E 4473392N
SiO_2	53.17	52.79	53.09	52.46	50.81	52.57	51.83	52.36	51.14	51.75	50.67	53.79	50.59	51.19	50.48	51.1
TiO_2	0.89	0.93	0.71	0.71	0.83	0.73	0.72	0.73	0.77	0.76	0.[illegible]9	0.75	0.77	0.78	0.8	0.78
Al_2O_3	17.78	18.09	18.68	18.39	16.32	20.02	20.12	19.94	21.05	20.46	2[illegible].05	20.82	20.91	19.13	21.54	21.04
$Fe_2O_3^*$	9.68	9.82	8.52	8.89	8.96	7.94	8.23	8.19	8.02	7.91	8.14	6.5	8.08	9.15	8.22	8.1
MnO	0.14	0.14	0.15	0.15	0.13	0.17	0.17	0.17	0.15	0.14	0.15	0.22	0.15	0.22	0.15	0.14
MgO	3.96	3.81	3.99	4.08	3.86	3.11	3.43	3.21	3.11	[illegible].01	3.15	2.56	3.07	4.71	3.07	3.04
CaO	5.33	6.13	7.85	7.28	5.14	8.42	8.52	9.15	10.[illegible]2	10.01	10.27	9.24	10.47	8.92	10.6	10.4
Na_2O	5.66	5.49	3.65	3.77	5.39	3.68	3.69	3.[illegible]23	2.85	2.71	2.8	3.47	2.73	3.13	2.79	2.75
K_2O	1.72	1.21	1.76	2.24	1.26	0.73	0.67	0.[illegible]1	0.13	0.1	0.1	0.88	0.09	0.3	0.1	0.09
P_2O_5	0.26	0.27	0.27	0.25	0.27	0.18	0.14	0.16	0.12	0.13	0.12	0.14	0.14	0.13	0.13	0.13
LOI	1.2	1.1	1.1	1.5	6.8	2.3	2.3	2.3	2.3	2.8	2.6	1.4	2.8	2.1	1.9	2.2
Sum	99.79	99.8	99.76	99.67	99.82	99.8	99.[illegible]	99.79	99.8	99.81	99.79	99.83	99.78	99.77	99.78	99.78
Ni	20.0	11.4	15.3	12.9	20.5	14	[illegible]1.1	21.3	14	12.5	11.7	5.2	5.4	4.5	5.2	4.6
Sc	24.0	24.0	20.0	20	22	[illegible]2	22	23	24	23	25	24	24	27	24	24
Ba	399.0	281.0	563	1292	26[illegible]	25[illegible]	268	190	155	137	157	266	127	258	129	133
Co	22.6	23.6	18.2	18.5	22.4	18.4	19.7	19.9	19.5	19.3	19.5	17	19.2	26	19.6	20
Hf	2.40	2.60	2.60	2.6	2.1	1.8	1.5	1.8	1.4	1.5	1.3	1.7	1.5	1.9	1.6	1.7
Nb	4.80	4.90	3.70	3.9	6	2.3	2	2.2	2.1	2.2	2.5	2.3	2.5	2.5	2.3	2.5
Rb	61.00	42.80	49.70	63.2	51	7.9	6.8	4.3	1.3	1	0.6	12.3	0.5	3.2	0.6	0.7
Sr	358	399	469	410.3	336.3	509.6	523.6	565.5	656.9	698.1	815.6	484.9	811	571	839.9	819
Ta	0.2	0.2	0.2	0.3	0.3	0.1		0.1	0.1	0.1				0.2		
Th	1.80	1.30	1.10	1.7	1.8	0.4	0.3	0.5	0.6	0.3	0.4	0.6	0.4	0.8	0.4	0.3
U	0.90	1.10	0.70	0.4	1.2			0.1				0.3		0.1	0.2	0.1
V	268	274	212	214	231	196	204	201	206	202	208	204	208	252	207	208
Zr	96.6	102.3	99.1	92.8	90.1	64.6	56.6	62	56.3	52.8	53.7	63	53.3	57.8	56.5	54.9
Y	23.5	24	22.6	19.8	22.5	21	19.3	18.7	17	16.8	17.5	15.3	16.6	15.5	16.6	18.2

Cu	48.4	15.7	23.1	109.9	44.6	128	140.6	128.2	106.8	105	99.8	30.1	110.3	51.8	101.9	108.4
Pb	4.20	4	4.20	11.8	3.5	6.3	3.8	3.9	3.1	3.2	3	1	3.3	2.7	2.9	3.3
Zn	40.0	33.0	25.0	54	31	49	41	37	41	42	42	40	37	28	38	34
La	14.50	16.00	17.7	17.4	15.6	8.6	7.6	8.5	6.2	6.4	7.4	7.7	6.4	7.5	7.1	6.7
Ce	32.60	33.30	37.5	36.5	30	18.9	17.1	18.3	15.3	15.4	16.6	17.3	15.9	17.4	16.8	15.4
Pr	4.15	4.14	4.32	4.34	3.83	2.63	2.23	2.47	2	1.98	2.11	2.15	2.1	2.17	2.21	2.11
Nd	16.90	18.70	18.3	16.5	18.5	11.8	10.3	12.4	9.7	9.6	9.8	8.7	9.2	9.4	10.8	9.6
Sm	3.84	4.64	3.76	4.25	3.83	3.4	2.76	2.98	2.69	2.4	2.5	2.41	2.46	2.28	2.67	2.49
Eu	1.19	1.21	1.25	1.22	1.05	1.15	1.01	1.1	0.92	0.87	0.94	0.87	0.88	0.91	0.95	0.89
Gd	4.32	4.62	3.92	3.99	4.3	3.54	3.19	3.36	2.96	2.92	3.17	2.84	2.82	2.72	3.07	2.89
Tb	0.71	0.74	0.67	0.63	0.67	0.58	0.55	0.59	0.49	0.5	0.53	0.47	0.51	0.43	0.49	0.52
Dy	4.17	4.25	3.65	3.93	3.85	3.67	3.22	3.55	3.21	2.76	2.91	3.01	3.13	2.97	3.16	2.96
Ho	0.89	0.94	0.77	0.81	0.92	0.79	0.73	0.78	0.67	0.73	0.65	0.62	0.59	0.59	0.71	0.65
Er	2.85	2.74	2.15	2.17	2.49	2.33	2.15	2.04	1.89	2.11	1.89	2.1	1.82	1.67	2.1	1.99
Tm	0.37	0.41	0.36	0.31	0.41	0.32	0.31	0.33	0.31	0.29	0.29	0.28	0.28	0.24	0.31	0.29
Yb	2.41	2.72	2.39	2.15	2.53	2.28	1.99	2.18	1.89	1.88	1.8	1.81	1.71	1.78	1.89	2.02
Lu	0.38	0.39	0.36	0.37	0.37	0.36	0.31	0.32	0.29	0.29	0.31	0.26	0.25	0.25	0.32	0.3
$(La/Yb)_N$	4.06	3.97	4.99	5.46	4.16	2.54	2.57	2.63	2.21	2.30	2.77	2.87	2.52	2.84	2.53	2.24
$(La/Lu)_N$	3.96	4.26	5.11	4.88	4.38	2.48	2.55	2.68	2.22	2.29	2.48	3.08	2.66	3.12	2.30	2.32
$(Dy/Yb)_N$	1.13	1.02	0.99	1.19	0.99	1.05	1.01	1.06	1.11	0.96	1.05	1.08	1.19	1.09	1.09	0.95
Eu/Eu*	0.89	0.79	0.99	0.89	0.79	1.01	1.04	1.06	0.99	1.00	1.04	1.01	1.02	1.12	1.01	1.01
Mg#	45	43	48	48	46	44	45	44	43	43	43	44	43	50	43	43

Note: $Fe_2O_3^{tot}$ = total iron as Fe_2O_3, LOI = loss on ignition, Eu/Eu* = (Eu_N) / 1/2 (Sm_N + Gd_N)) and Mg# (Mg-number)= 100 x MgO / ($MgO+0.9Fe_2O_3^{tot}$)

Tablo 3.

Sample	U-Pb (Ma)	Rb (ppm)	Sr (ppm)	Pb (ppm)	$^{87}Rb/^{86}Sr$	$^{87}Sr/^{86}Sr$	2s	I_{sr}	Sm (ppm)	Nd (ppm)	$^{147}Sm/^{144}Nd$	$^{143}Nd/^{144}Nd$	$(^{143}Nd/^{144}Nd)_i$	2s	$\varepsilon_{Nd}(0)$	$\varepsilon_{Nd}(T)$	T_{DM} (Ma)	$^{206}Pb/^{204}Pb$	$^{207}Pb/^{204}Pb$	$^{208}Pb/^{204}Pb$
A-SPD																				
B48	46	0.60	840.0	2.9	0.002	0.70481	10	0.70481	2.67	10.80	0.1501	0.51263	0.51259	4	-0.1	0.2	1148	18.512	15.573	38.485
B42	46	12.30	485.0	1.0	0.073	0.70487	11	0.70482	2.41	8.70	0.1682	0.51264	0.51259	6	0.0	0.2	1531	18.520	15.574	38.496
B24	46	1.00	698.0	3.2	0.004	0.70482	10	0.70481	2.40	9.60	0.1518	0.51263	0.51258	9	-0.2	0.1	1186	18.527	15.581	38.510
B2	46	7.90	510.0	6.3	0.045	0.70451	10	0.70448	3.40	11.80	0.1750	0.51273	0.51268	5	1.9	2.0	1445	18.447	15.556	38.422
B44	46	3.20	571.0	2.7	0.016	0.70481	12	0.70480	2.28	9.40	0.1473	0.51266	0.51261	7	0.4	0.7	1048	18.497	15.576	38.507
H-SPD																				
B37	46	49.70	469.0	4.2	0.307	0.70536	10	0.70516	3.76	18.30	0.1248	0.51264	0.51264	4	0.7	1.2	769	18.431	15.587	38.552
B32	46	63.20	410.0	11.8	0.446	0.70571	12	0.70542	4.25	16.50	0.1564	0.51269	0.51264	8	0.9	1.2	1134	18.714	15.658	38.807

Note: $\varepsilon_{Nd} = (((^{143}Nd/^{144}Nd)_s/(^{143}Nd/^{144}Nd)_{CHUR} - 1) \times 10000$. $f_{Sm/Nd} = (^{147}Sm/^{144}Sm)_s/(^{147}Sm/^{144}Sm)_{CHUR} - 1$. $(^{143}Nd/^{144}Nd)_{CHUR} = 0.512638$ and $(^{147}Sm/^{144}Sm)_{CHUR} = 0.1967$

The model ages were calculated using a linear isotopic ratio growth equation: $T_{DM} = 1/l \times \ln(1 + ((^{143}Nd/^{144}Nd)_s - 0.51315)/((^{147}Sm/^{144}Nd)_s - 0.2137))$.

CHUR: Chondritic Uniform Reservoir; DM: depleted mantle. i: initial.

Table 4.

Mantle Sources	Modal proportions				Normative weight fractions of minerals (i) in the partial melts
Garnet lherzolite	$Ol_{0.598}Opx_{0.211}Cpx_{0.076}Grt_{0.115}$				$Ol_{0.05}Opx_{0.2}Cpx_{0.3}Grt_{0.45}$
Spinel lherzolite	$Ol_{0.578}Opx_{0.27}Cpx_{0.119}Spl_{0.033}$				$Ol_{0.1}Opx_{0.27}Cpx_{0.5}Spl_{0.13}$
Garnet-amphibole-spinel lherzolite	$Ol_{0.55}Opx_{0.2}Cpx_{0.15}Grt_{0.05}Amp_{0.04}Phl_{0.01}$				$Ol_{0.05}Opx_{0.05}Cpx_{0.2}Grt_{0.2}Amp_{0.04}Phl_{0.1}$
Partition coefficients	Dy	La	Sm	Yb	Partition coefficient (*D*) values are from Keskin (1994). McKenzie and O'Nions (1991. 1995) and GERM (Geochemical Earth Reference Model) website. at http://earthref.org/databases/KDD/
Olivine	0.0017	0.0004	0.0013	0.0015	
Orthopyroxene	0.022	0.002	0.01	0.049	Source compositions: Primitive mantle REE composition (McDonough and Sun. 1995) was chosen for all partial melting scenarios
Clinopyroxene	0.33	0.0435	0.26	0.313	
Garnet	1.06	0.01	0.217	4.3	Ol: olivine. Opx: orthopyroxene. Cpx: clinopyroxene. Grt: garnet. Spl: spinel. Amp: amphibole. Phl: phlogopite
Spinel	0.01	0.01	0.01	0.01	
Amphibole	0.78	0.2	0.76	0.8	Garnet and spinel lherzolite composition are from Thirlwall et al. (1994). Garnet-amphibole-phlogopite lherzolite is from Barry et al 2003.
Phlogopite	0.03	0.35	0.031	0.04	

Table 5

Magma Composition	Elements	Olivine	Clinopyroxene	Plagioclase	Amphibole	Biotite	Magnetite
Basic	Co	5.9	2	0.07	2	23	7.4
	Th	0.04	0.03	0.01	0.05	0.0145	-

Kd values of Rb. Sc. Sr. Nb. Dy and Sr for amphibole. plagioclase. clinopyroxene. olivine. biotite and sanidine were compiled from Rollinson (1993). GERM Partition Coefficient (Kd) Database of Earth Reference Data and Models website (http://earthref.org/; see the references therein) and Keskin (2002).

Table 6

	Sr (ppm)	$^{87}Sr/^{86}Sr$	Nd (ppm)	εNd	Pb (ppm)	$^{206}Pb/^{204}Pb$
UM	20	0.703	1.2	8	0.185	18
Lower Crust	300	0.710	24	-30	4.2	15.518
Upper Crust	350	0.718	26	-25	30	19

UMstands for upper mantle peridotite. Sr–Nd data of UMare fromJahn et al. (1999).PbdataarefromSun and McDonough (1989).Sr–Nd data of the lower crust are fromXu et al. (2004) and Jahn et al. (1999). Pb isotopic composition is from Zhang (1995). Pb concentration is from Rudnick and Fountain (1995).Sr–Nd data of the upper crust are from Xu et al. (2004).Pbisotopic composition is from Wang et al. (2005).

CRediT authorship contribution statement

Emre Aydınçakır: Conceptualization, writing - original draft, Writing - review & editing. **Cem Yücel:** Methodology, Writing -review & editing. **Gilles Ruffet:** Data curation, Methodology. **Mehmet Ali Gücer:** Software, field study. **Enver Akaryalı**: field study. **Abdullah Kaygusuz**: review & editing, Methodology.

Declaration of interests

☒ The authors declare that they have no known competing financial interests or personal relationships that could have appeared to influence the work reported in this paper.

☐The authors declare the following financial interests/personal relationships which may be considered as potential competing interests:

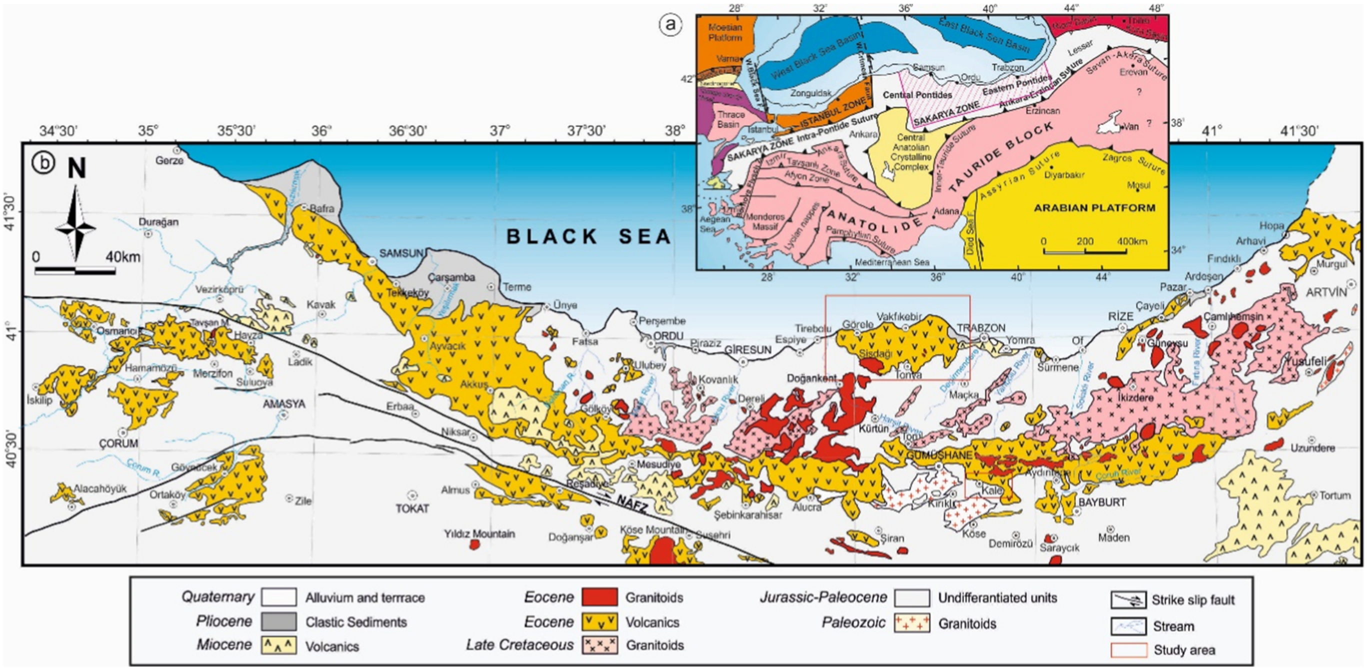
a
b
N
0
40km
BLACK SEA
Quaternary
Alluvium and terrace
Pliocene
Clastic Sediments
Miocene
Volcanics
Eocene
Granitoids
Eocene
Volcanics
Late Cretaceous
Granitoids
Jurassic-Paleocene
Undifferantiated units
Paleozoic
Granitoids
Strike slip fault
Stream
Study area
SAMSUN
TRABZON
GİRESUN
ORDU
RİZE
ARTVİN
GÜMÜŞHANE
BAYBURT
AMASYA
TOKAT
ÇORUM
NAFZ
ARABIAN PLATFORM
TAURIDE BLOCK
ANATOLIDE

Figure 1

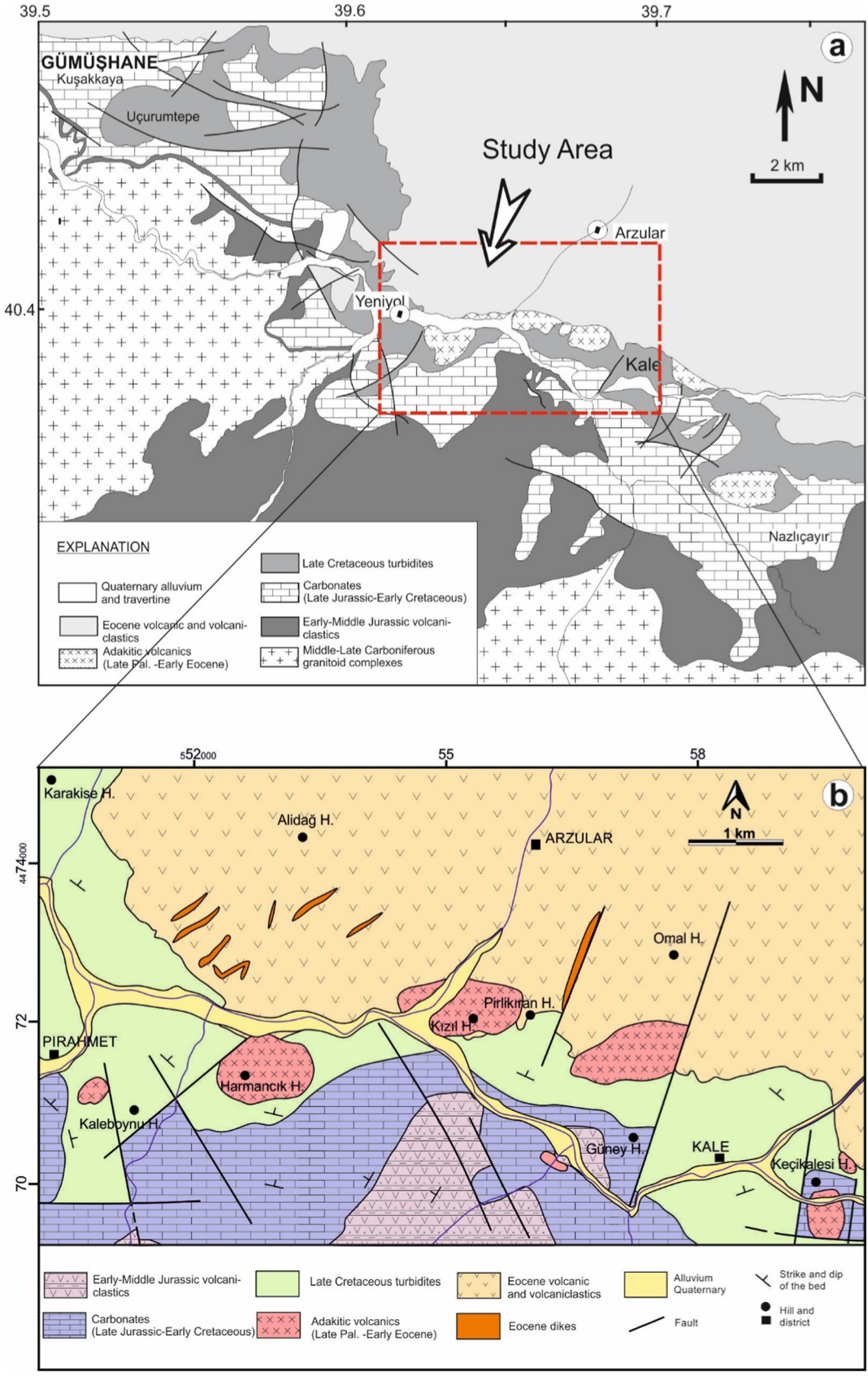
39.5
39.6
39.7
40.4
a
GÜMÜŞHANE
Kuşakkaya
Uçurumtepe
Study Area
N
2 km
Arzular
Yeniyol
Kale
Nazlıçayır
EXPLANATION
Quaternary alluvium and travertine
Eocene volcanic and volcani-clastics
Adakitic volcanics (Late Pal. -Early Eocene)
Late Cretaceous turbidites
Carbonates (Late Jurassic-Early Cretaceous)
Early-Middle Jurassic volcani-clastics
Middle-Late Carboniferous granitoid complexes
552000
55
58
4474000
72
70
b
Karakise H.
Alidağ H.
ARZULAR
N
1 km
Omal H.
Pirlıkıran H.
Kızıl H.
PIRAHMET
Harmancık H.
Kalebeynu H.
Güney H.
KALE
Keçikalesi H.
Early-Middle Jurassic volcani-clastics
Late Cretaceous turbidites
Eocene volcanic and volcaniclastics
Alluvium Quaternary
Strike and dip of the bed
Carbonates (Late Jurassic-Early Cretaceous)
Adakitic volcanics (Late Pal. -Early Eocene)
Eocene dikes
Fault
Hill and district

Figure 2

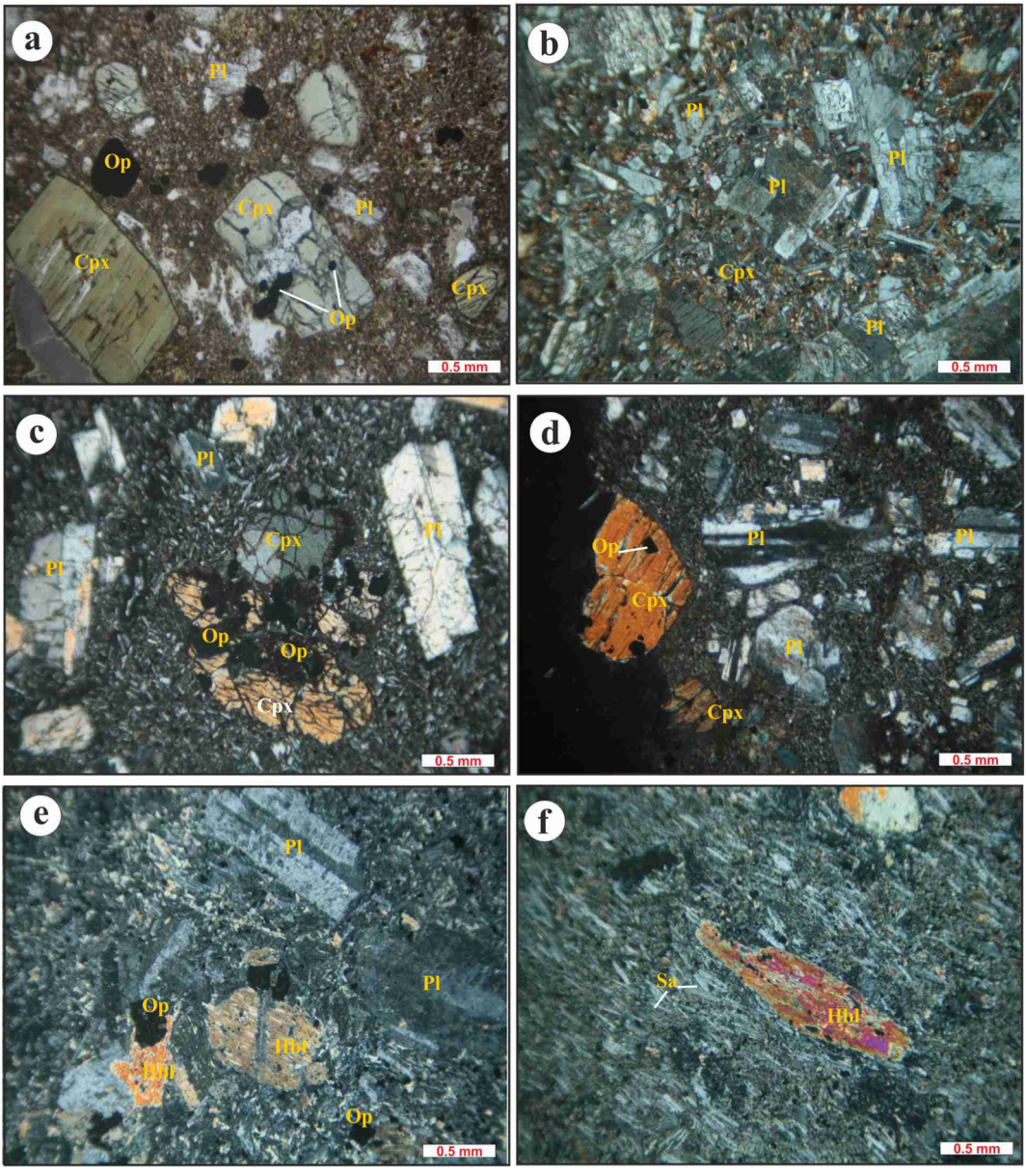
a
Pl
Op
Cpx
Pl
Cpx
Cpx
Op
0.5 mm
b
Pl
Pl
Pl
Cpx
Pl
0.5 mm
c
Pl
Cpx
Pl
Pl
Op
Op
Cpx
0.5 mm
d
Op
Pl
Pl
Cpx
Pl
Cpx
0.5 mm
e
Pl
Pl
Op
Hbl
Hbl
Op
0.5 mm
f
Sa
Hbl
0.5 mm

Figure 3

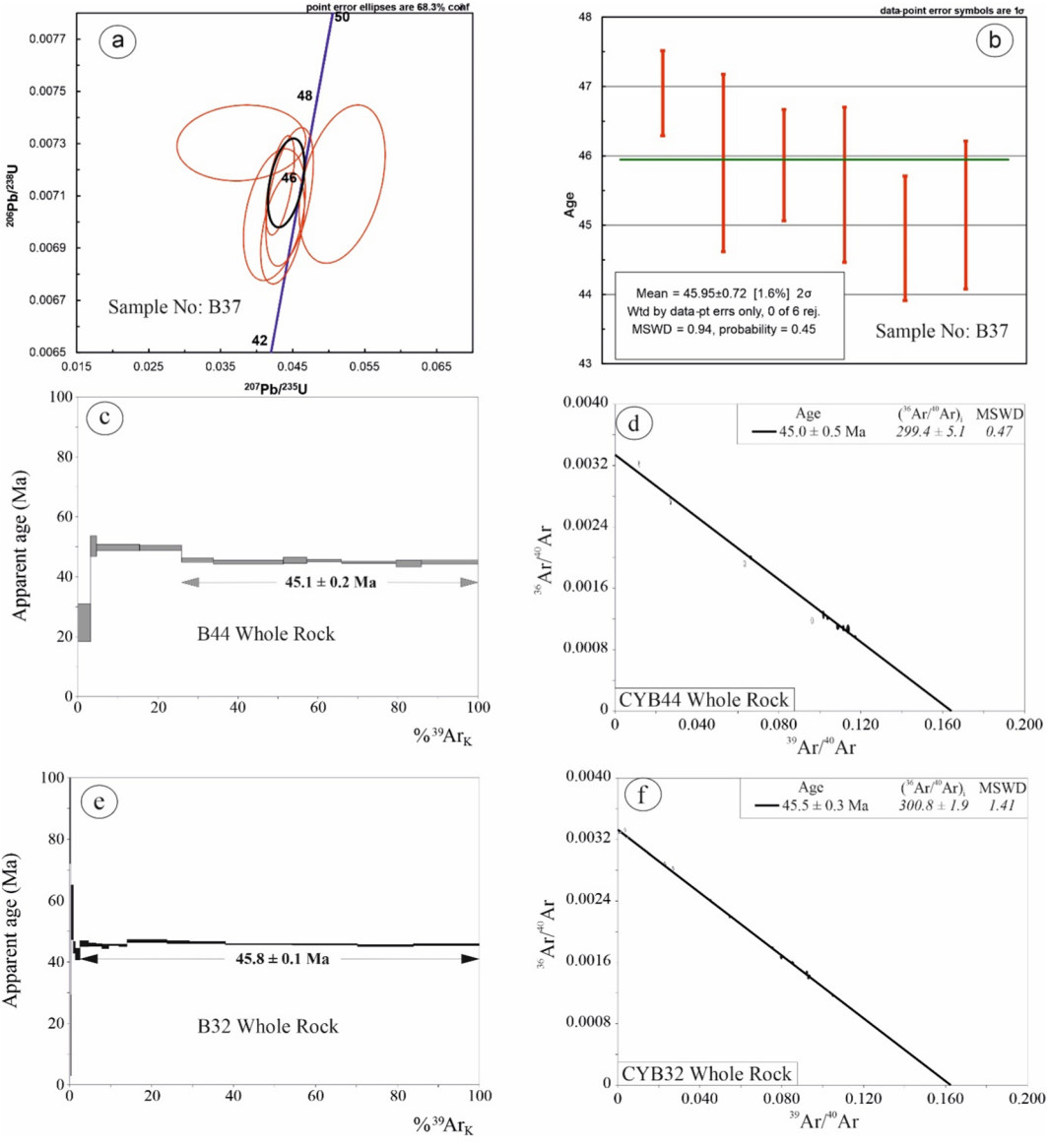
a
point error ellipses are 68.3% conf
50
48
46
42
Sample No: B37
$^{206}Pb/^{238}U$
$^{207}Pb/^{235}U$
b
data-point error symbols are 1σ
Age
Mean = 45.95±0.72 [1.6%] 2σ
Wtd by data-pt errs only, 0 of 6 rej.
MSWD = 0.94, probability = 0.45
Sample No: B37
c
Apparent age (Ma)
45.1 ± 0.2 Ma
B44 Whole Rock
$\%^{39}Ar_K$
d
Age
$(^{36}Ar/^{40}Ar)_i$
MSWD
45.0 ± 0.5 Ma
299.4 ± 5.1
0.47
$^{36}Ar/^{40}Ar$
CYB44 Whole Rock
$^{39}Ar/^{40}Ar$
e
Apparent age (Ma)
45.8 ± 0.1 Ma
B32 Whole Rock
$\%^{39}Ar_K$
f
Age
$(^{36}Ar/^{40}Ar)_i$
MSWD
45.5 ± 0.3 Ma
300.8 ± 1.9
1.41
$^{36}Ar/^{40}Ar$
CYB32 Whole Rock
$^{39}Ar/^{40}Ar$

Figure 4

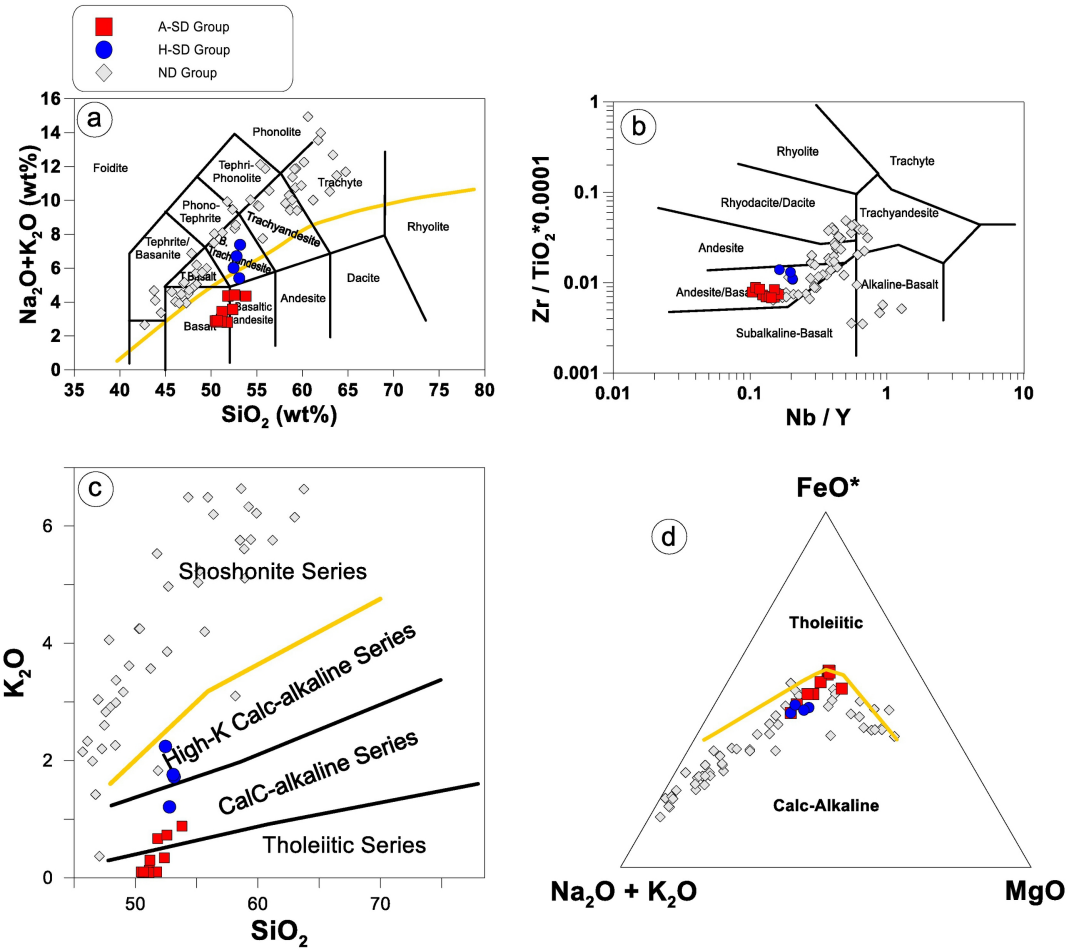
A-SD Group
H-SD Group
ND Group
a
Foidite
Phonolite
Tephri-Phonolite
Trachyte
Phono-Tephrite
Trachyandesite
Rhyolite
Tephrite/ Basanite
B. Trachyandesite
Basalt
Dacite
Andesite
Basaltic Andesite
Basalt
Na2O+K2O (wt%)
SiO2 (wt%)
b
Rhyolite
Trachyte
Rhyodacite/Dacite
Trachyandesite
Andesite
Andesite/Basalt
Alkaline-Basalt
Subalkaline-Basalt
Zr / TiO2*0.0001
Nb / Y
c
Shoshonite Series
High-K Calc-alkaline Series
CalC-alkaline Series
Tholeiitic Series
K2O
SiO2
d
FeO*
Tholeiitic
Calc-Alkaline
Na2O + K2O
MgO

Figure 5

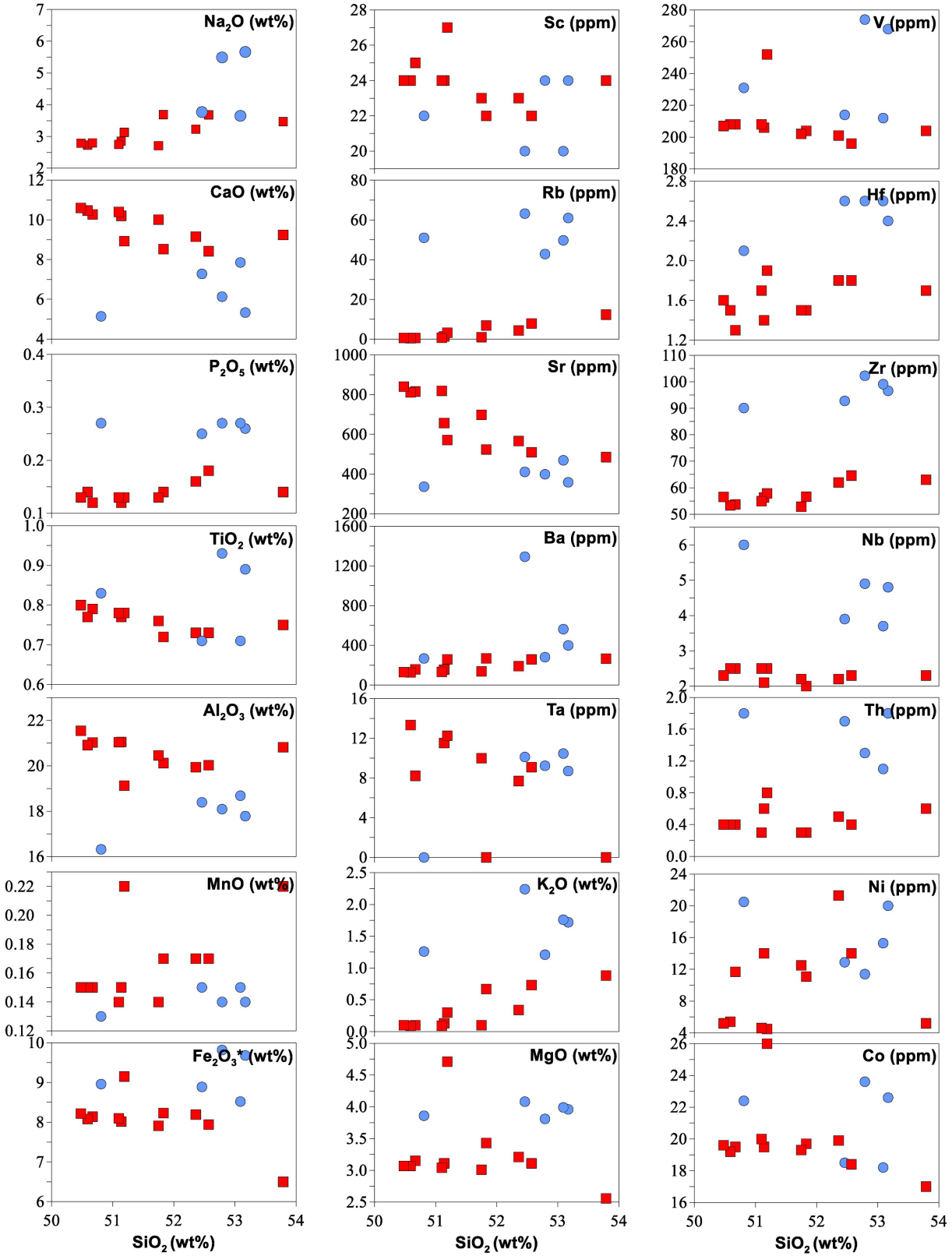
Na2O (wt%)
Sc (ppm)
V (ppm)
CaO (wt%)
Rb (ppm)
Hf (ppm)
P2O5 (wt%)
Sr (ppm)
Zr (ppm)
TiO2 (wt%)
Ba (ppm)
Nb (ppm)
Al2O3 (wt%)
Ta (ppm)
Th (ppm)
MnO (wt%)
K2O (wt%)
Ni (ppm)
Fe2O3* (wt%)
MgO (wt%)
Co (ppm)
SiO2 (wt%)
SiO2 (wt%)
SiO2 (wt%)

Figure 6

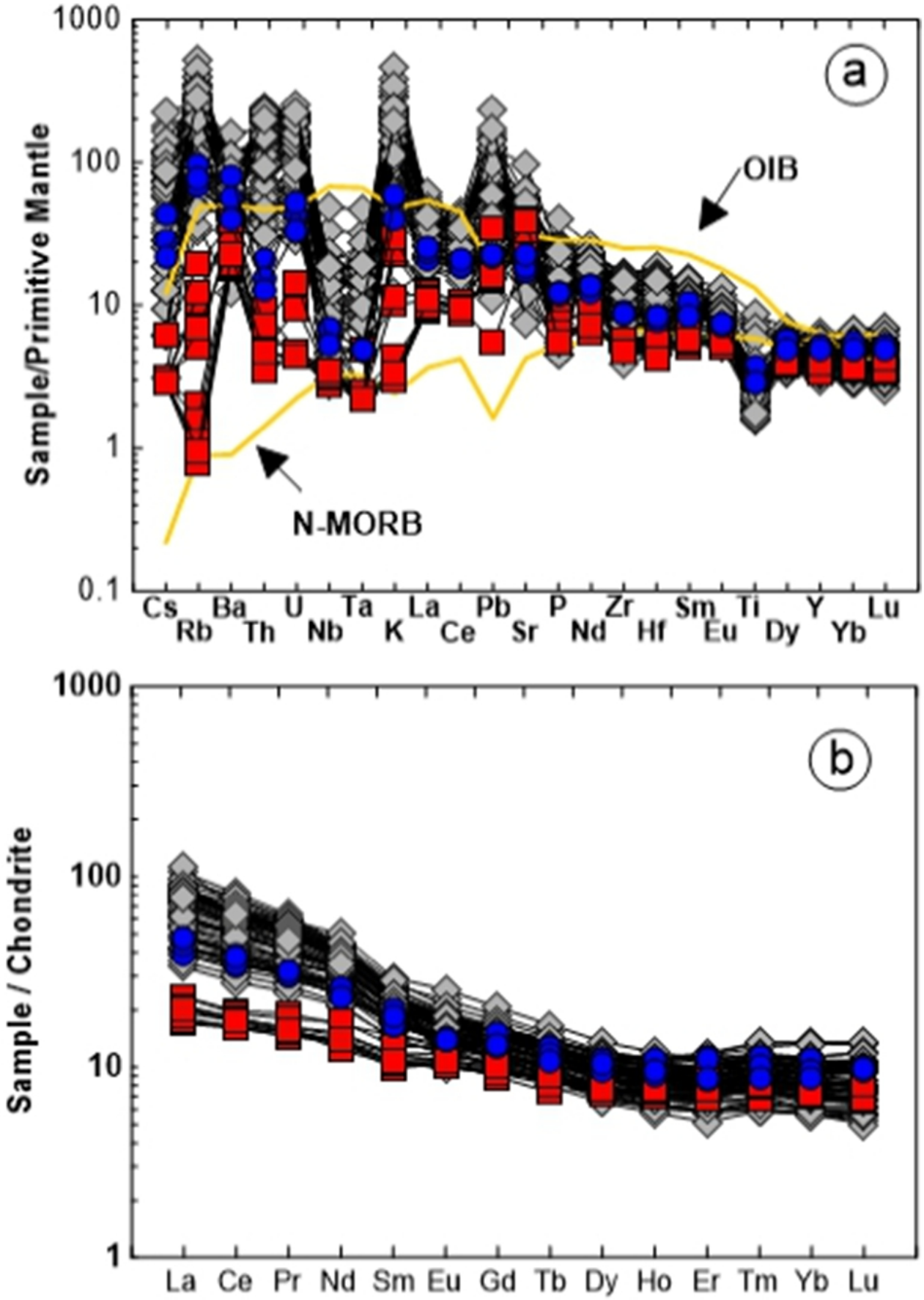
a
Sample/Primitive Mantle
1000
100
10
1
0.1
OIB
N-MORB
Cs Rb Ba Th U Nb Ta K La Ce Pb Sr P Nd Zr Hf Sm Eu Ti Dy Y Yb Lu
b
Sample / Chondrite
1000
100
10
1
La Ce Pr Nd Sm Eu Gd Tb Dy Ho Er Tm Yb Lu

Figure 7

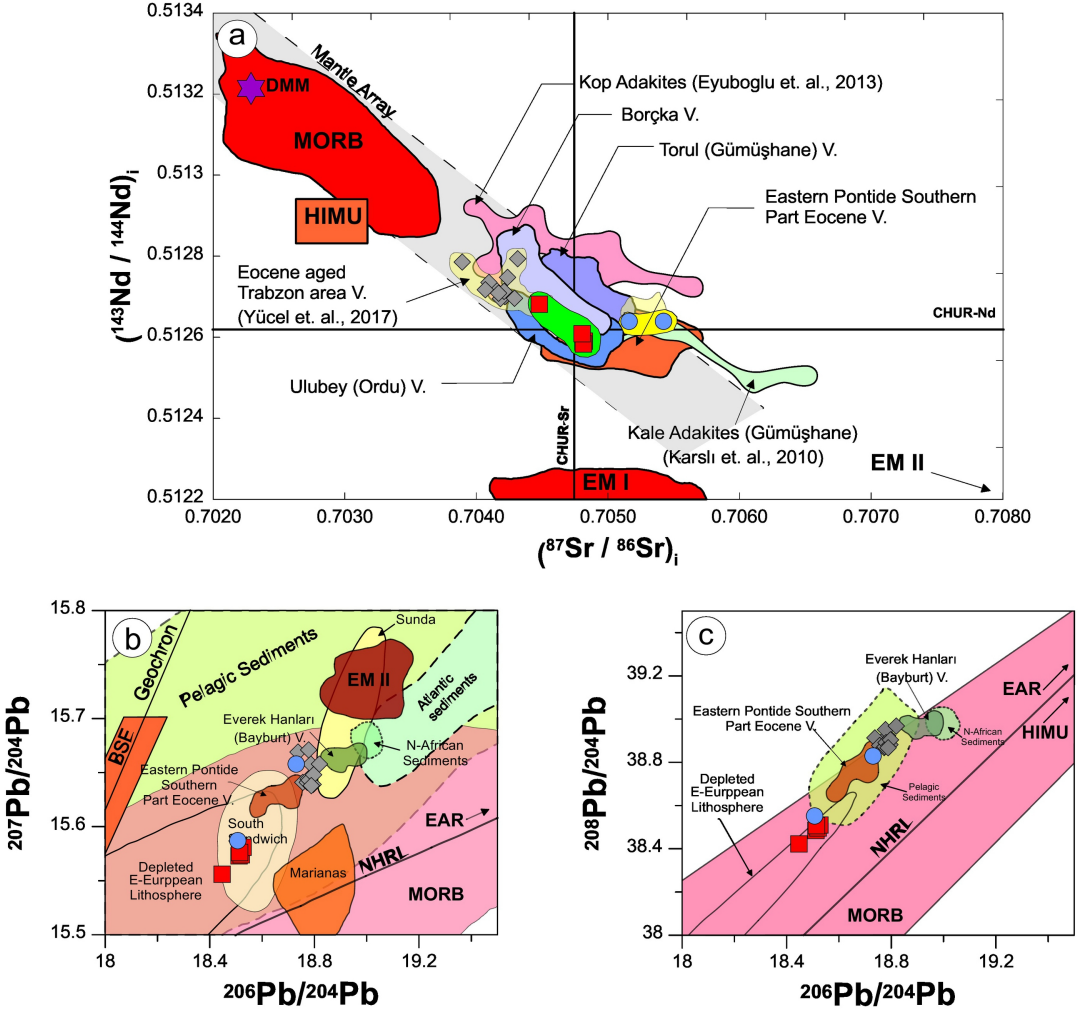
a
Mantle Array
DMM
MORB
HIMU
Kop Adakites (Eyuboglu et. al., 2013)
Borçka V.
Torul (Gümüşhane) V.
Eastern Pontide Southern Part Eocene V.
Eocene aged Trabzon area V. (Yücel et. al., 2017)
CHUR-Nd
Ulubey (Ordu) V.
CHUR-Sr
Kale Adakites (Gümüşhane) (Karslı et. al., 2010)
EM I
EM II
0.5134
0.5132
0.513
0.5128
0.5126
0.5124
0.5122
0.7020
0.7030
0.7040
0.7050
0.7060
0.7070
0.7080
(143Nd / 144Nd)i
(87Sr / 86Sr)i
b
Geochron
Pelagic Sediments
Sunda
EM II
Atlantic sediments
Everek Hanları (Bayburt) V.
N-African Sediments
BSE
Eastern Pontide Southern Part Eocene V.
South Sandwich
EAR
Depleted E-Eurppean Lithosphere
Marianas
NHRL
MORB
15.8
15.7
15.6
15.5
18
18.4
18.8
19.2
207Pb/204Pb
206Pb/204Pb
c
Everek Hanları (Bayburt) V.
EAR
Eastern Pontide Southern Part Eocene V.
N-African Sediments
HIMU
Depleted E-Eurppean Lithosphere
Pelagic Sediments
NHRL
MORB
39.2
38.8
38.4
38
18
18.4
18.8
19.2
208Pb/204Pb
206Pb/204Pb

Figure 8

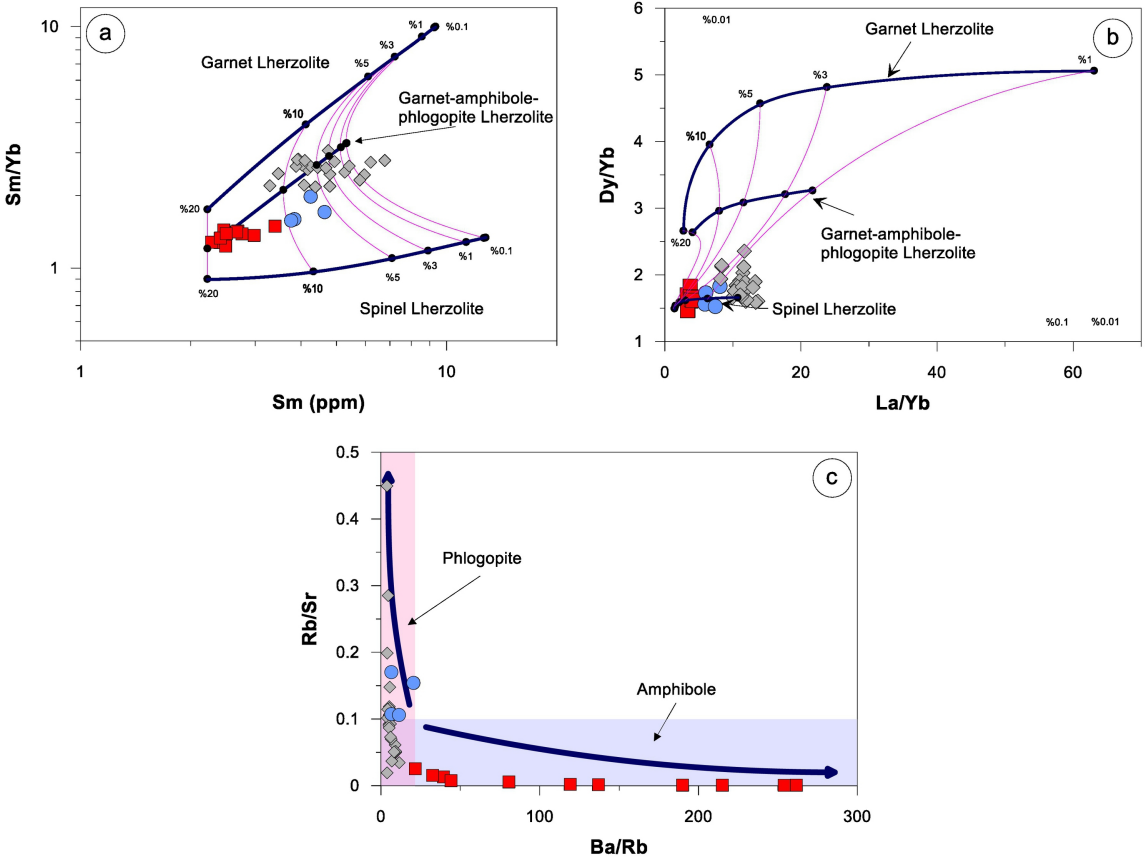
a
Garnet Lherzolite
Garnet-amphibole-
phlogopite Lherzolite
Spinel Lherzolite
%1
%0.1
%3
%5
%10
%20
Sm/Yb
Sm (ppm)
10
1
b
Garnet Lherzolite
Garnet-amphibole-
phlogopite Lherzolite
Spinel Lherzolite
%0.01
%0.1
Dy/Yb
La/Yb
6
5
4
3
2
1
0
20
40
60
c
Phlogopite
Amphibole
Rb/Sr
Ba/Rb
0.5
0.4
0.3
0.2
0.1
0
100
200
300

Figure 9

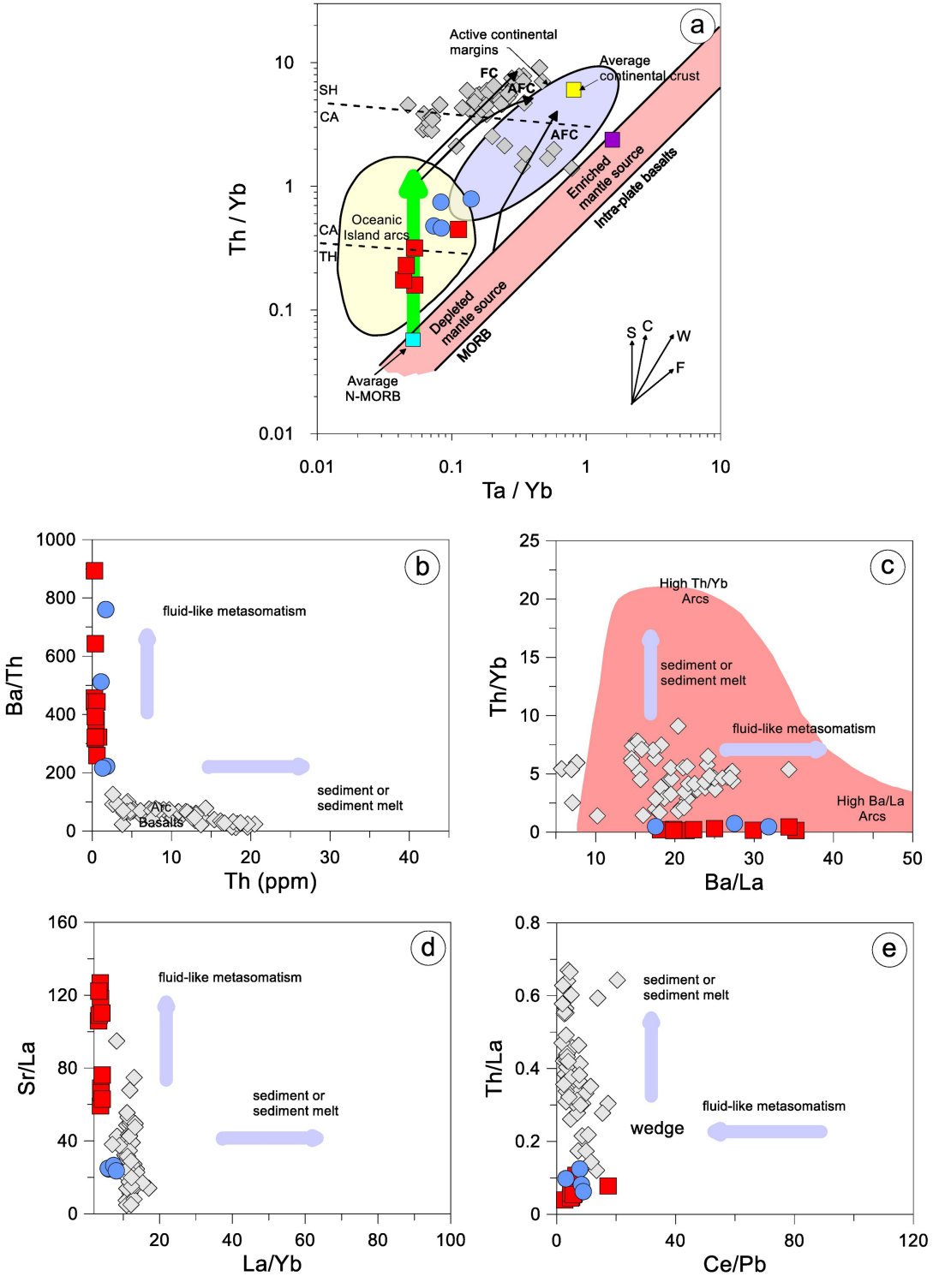
a
Active continental margins
FC
AFC
Average continental crust
SH
CA
AFC
Enriched mantle source
Intra-plate basalts
Oceanic Island arcs
CA
TH
Depleted mantle source
MORB
Avarage N-MORB
S
C
W
F
Th / Yb
Ta / Yb
0.01
0.1
1
10
b
fluid-like metasomatism
sediment or sediment melt
Arc Basalts
Ba/Th
Th (ppm)
0
200
400
600
800
1000
0
10
20
30
40
c
High Th/Yb Arcs
sediment or sediment melt
fluid-like metasomatism
High Ba/La Arcs
Th/Yb
Ba/La
0
5
10
15
20
25
10
20
30
40
50
d
fluid-like metasomatism
sediment or sediment melt
Sr/La
La/Yb
0
40
80
120
160
20
40
60
80
100
e
sediment or sediment melt
fluid-like metasomatism
wedge
Th/La
Ce/Pb
0
0.2
0.4
0.6
0.8
0
40
80
120

Figure 10

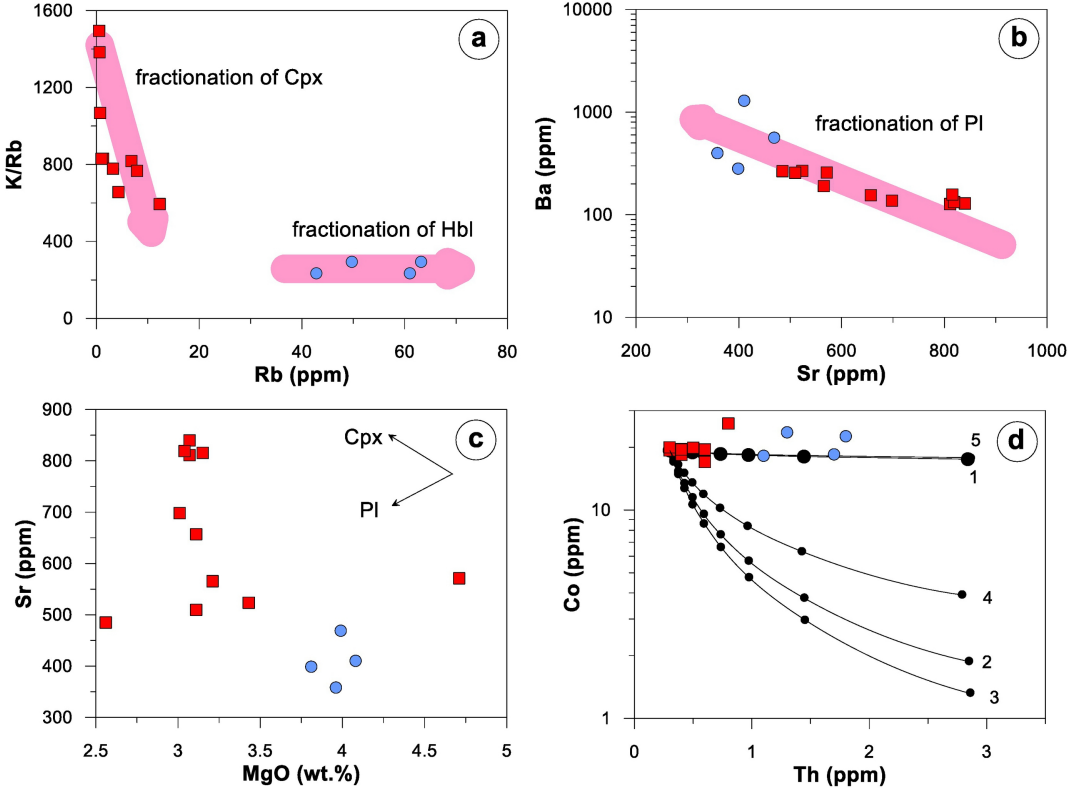
a
fractionation of Cpx
fractionation of Hbl
K/Rb
Rb (ppm)
b
fractionation of Pl
Ba (ppm)
Sr (ppm)
c
Cpx
Pl
Sr (ppm)
MgO (wt.%)
d
5
1
4
2
3
Co (ppm)
Th (ppm)

Figure 11

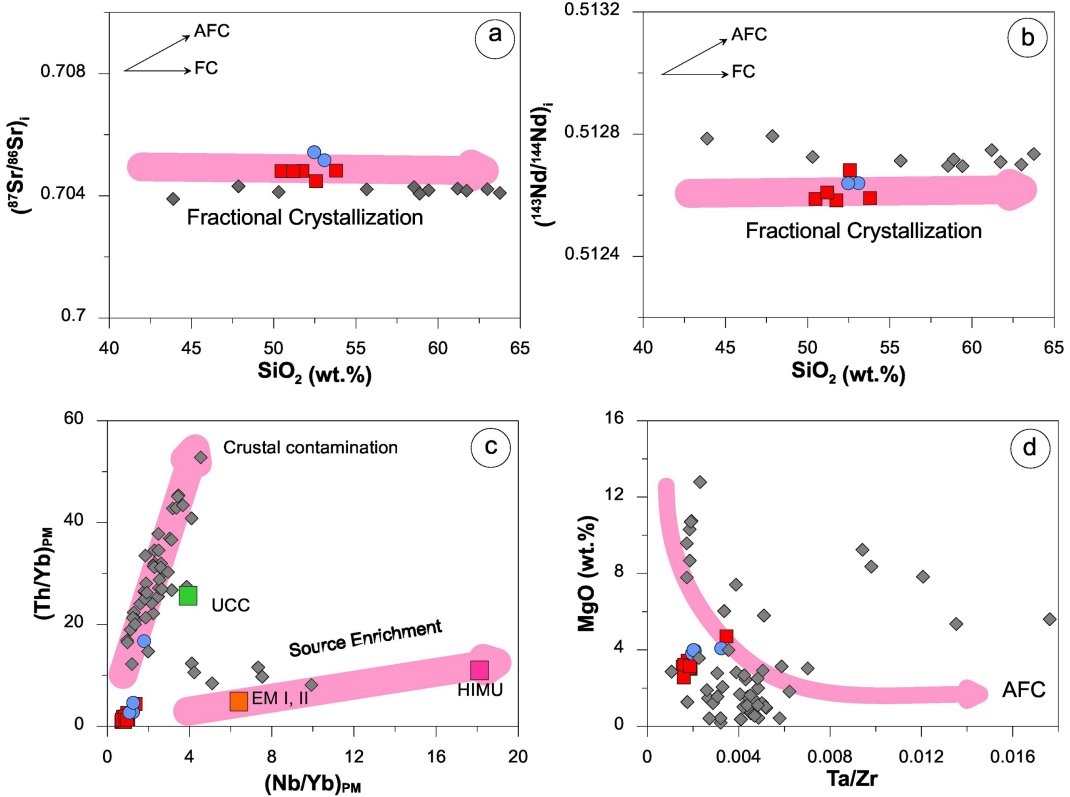
a
AFC
FC
0.708
0.704
0.7
$(^{87}Sr/^{86}Sr)_i$
Fractional Crystallization
40
45
50
55
60
65
SiO_2 (wt.%)
b
0.5132
0.5128
0.5124
$(^{143}Nd/^{144}Nd)_i$
c
Crustal contamination
UCC
Source Enrichment
EM I, II
HIMU
$(Th/Yb)_{PM}$
$(Nb/Yb)_{PM}$
d
MgO (wt.%)
AFC
Ta/Zr
0.004
0.008
0.012
0.016

Figure 12

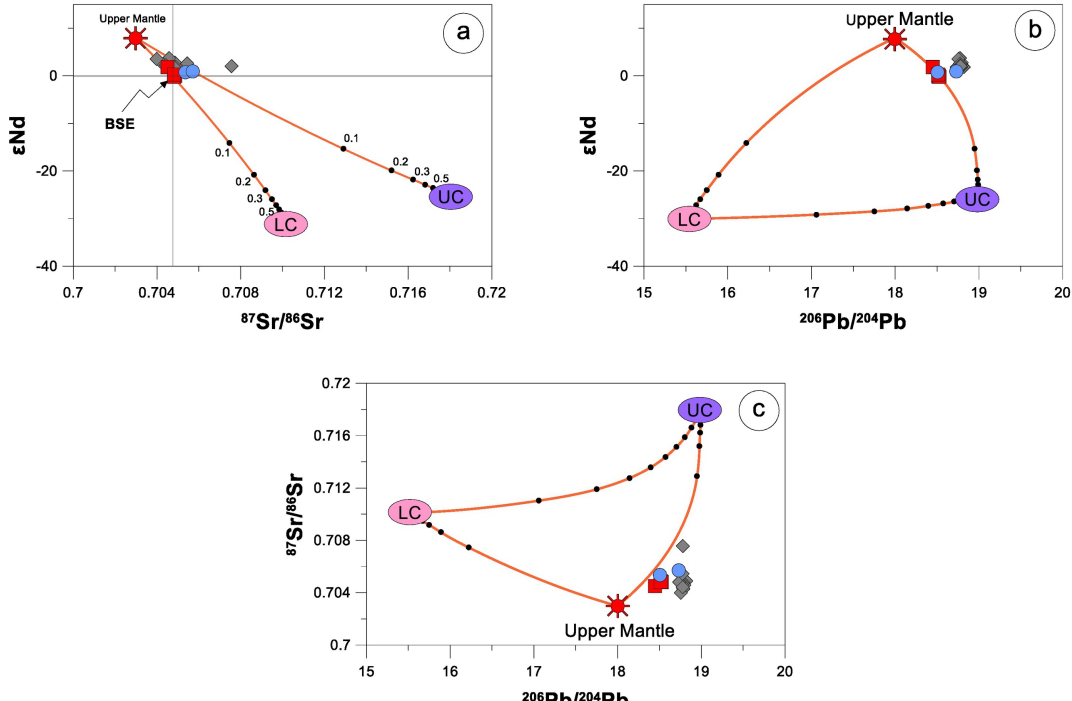
a
Upper Mantle
BSE
εNd
0
-20
-40
0.7
0.704
0.708
0.712
0.716
0.72
87Sr/86Sr
0.1
0.2
0.3
0.5
LC
UC
b
Upper Mantle
εNd
15
16
17
18
19
20
206Pb/204Pb
c
87Sr/86Sr
Upper Mantle

Figure 13